miRNA-mediated control of gephyrin synthesis drives sustained inhibitory synaptic plasticity

Theresa M. Welle[1,2], Dipen Rajgor[1,2], Joshua D. Garcia[1], Dean Kareemo[1], Sarah M. Zych[1], Sara E. Gookin[1], Tyler P. Martinez[1], Mark L. Dell'Acqua[1], Christopher P. Ford[1], Matthew J. Kennedy[1], Katharine R. Smith[1*].

[1]Department of Pharmacology, University of Colorado School of Medicine, Anschutz Medical Campus, 12800 East 19th Avenue, Aurora, CO 80045.

[2]T.M.W and D.R. contributed equally to this work.

[*]Corresponding author: katharine.r.smith@cuanschutz.edu.

ABSTRACT

Activity-dependent protein synthesis is crucial for many long-lasting forms of synaptic plasticity. However, our understanding of the translational mechanisms controlling inhibitory synapses is limited. One distinct form of inhibitory long-term potentiation (iLTP) enhances postsynaptic clusters of $GABA_A$Rs and the primary inhibitory scaffold, gephyrin, to promote sustained synaptic strengthening. While we previously found that persistent iLTP requires mRNA translation, the precise mechanisms controlling gephyrin translation during this process remain unknown. Here, we identify miR153 as a novel regulator of *Gphn* mRNA translation which controls gephyrin protein levels and synaptic clustering, ultimately impacting GABAergic synaptic structure and function. We find that iLTP induction downregulates miR153, reversing its translational suppression of *Gphn* mRNA and allowing for increased *de novo* gephyrin protein synthesis and synaptic clustering during iLTP. Finally, we find that reduced miR153 expression during iLTP is driven by an excitation-transcription coupling pathway involving calcineurin, NFAT and HDACs, which also controls the miRNA-dependent upregulation of $GABA_A$Rs. Overall, this work delineates a miRNA-dependent post-transcriptional mechanism that controls the expression of the key synaptic scaffold, gephyrin, and may converge with parallel miRNA pathways to coordinate gene upregulation to maintain inhibitory synaptic plasticity.

INTRODUCTION

Activity-dependent, long-term changes in excitatory and inhibitory synaptic strength are crucial for tuning neural excitability, sculpting networks, and supporting higher order brain functions involved in learning, memory, and cognition.[1,2] Synaptic function and plasticity are supported by continuous changes in gene expression via processes like transcription and translation to alter the synaptic proteome. Indeed, mRNA translation is essential for many different forms of plasticity and particularly critical for shaping synaptic strength long-term. [3-11] Although there is a wealth of research uncovering how translation facilitates long-term plasticity of glutamatergic synapses,[11-13] our understanding of its contribution to activity-dependent changes in GABAergic synaptic strength remains limited. Synaptic inhibition modulates excitatory plasticity and circuit firing, maintaining an appropriate level of neural activity via excitatory/inhibitory (E/I) balance.[14,15] Therefore, understanding how activity-dependent changes in gene expression contribute to long-term inhibitory synaptic strength is imperative for a complete view of brain function.

In the central nervous system, synaptic inhibition is primarily mediated by GABAergic synapses, where GABA type A receptors ($GABA_A$Rs) are clustered opposite GABA-releasing presynaptic terminals by the principal scaffold, gephyrin.[16-21] Gephyrin plays a crucial role in GABAergic synaptic function and plasticity, and its disruption is associated with neuropathologies including epilepsy and Alzheimer's disease.[22-30] GABAergic synapses can undergo numerous forms of bidirectional plasticity to strengthen or weaken synaptic inhibition, thus impacting neuronal excitability.[31-33] An important form of plasticity is inhibitory long-term potentiation (iLTP), which is mediated by NMDA receptor (NMDAR) activity[10,34-37] driving heterosynaptic changes at GABAergic postsynapses. Given the importance of iLTP for controlling excitatory potentiation[38-40] and its role in learning and sensory experience *in vivo*,[40,41] it is crucial to understand the underlying mechanisms driving this process.

Previous work found that the strengthening of inhibitory synapses during iLTP is primarily driven by increased postsynaptic clustering of $GABA_A$Rs and gephyrin.[10,34-36] In the first 20-30 min, this clustering is accommodated by recruitment of pre-existing proteins.[10,36] However, we recently showed that to sustain iLTP over longer timescales, translation of GABAergic synaptic components is required.[10] Following iLTP induction, translational repression of *Gabra1* and *Gabrg2* mRNAs, encoding synaptic $GABA_A$R subunits α1 and γ2, is relieved to enable *de novo* synthesis and increased $GABA_A$R synaptic clustering. We found that this mechanism is mediated by the microRNA, miR376c. MicroRNAs (miRNA) are key regulators of activity-dependent translation in neurons, where they control expression of numerous synaptic genes.[42-45] However, the mechanisms driving translation of gephyrin, the critical inhibitory scaffold, remain unknown. In this work, we aimed to characterize these mechanisms which control gephyrin translation and its upregulation during iLTP.

Here we identify miR153 as a novel regulator of gephyrin mRNA (*Gphn*) translation in neurons and find that its downregulation is critical for sustaining GABAergic synaptic clustering during iLTP. Following iLTP stimulation, miR153 expression is reduced, allowing *Gphn* translation, and the subsequent increase of gephyrin and $GABA_A$R clusters at inhibitory synapses. Remarkably, we find that miR153 is transcriptionally repressed following iLTP stimulation, a process that is controlled by the same signaling pathway regulating miR376c expression during iLTP. Together, our findings provide a mechanism by which iLTP stimulation can induce signaling to coordinate the downregulation of miR376c and miR153 concurrently, thereby modulating the expression of their targets (*Gabra1*, *Gabrg2* and *Gphn*), which are essential for potentiating synaptic inhibition.

RESULTS

miR153 regulates *Gphn* translation during iLTP

To investigate whether gephyrin mRNA translation could be controlled by miRNA activity during iLTP, we treated cultured hippocampal neurons with an extensively characterized iLTP protocol (20 μM NMDA, 10 μM CNQX for 2 min) which augments inhibitory synaptic transmission,[10,34-36] and is sustained for at least 90 min post-stimulation.[10] At 90 min following iLTP or sham stimulation we performed Argonaute 2 (AGO2) immunoprecipitation assays. AGO2 is part of the RNA-Induced Silencing Complex (RISC), which is crucial for miRNA-mediated translational repression (Fig. 1A). When a transcript is bound to AGO2, this indicates its incorporation into the RISC in which translation of the mRNA is likely regulated by miRNAs. Thus, the proportion of AGO2-bound mRNA can indicate the extent of miRNA-mediated translational control. AGO2 was immunoprecipitated from control and iLTP-treated neurons, and we used qRT-PCR to measure AGO2-bound *Gphn* (Fig. S1A,B). Following iLTP stimulation, we observed reduced binding of *Gphn* mRNA by AGO2 compared to control conditions, suggesting some alleviation of miRNA-mediated translational suppression during iLTP. Furthermore, total *Gphn* levels were unchanged following stimulation, confirming that elevated gephyrin expression during iLTP is not likely due to increased transcription (Fig. S1C).

To identify miRNAs that might mediate *Gphn* silencing, we cross-referenced miRNA seed sites in the *Gphn* 3'UTR (identified by TargetScan and miRDB)[46,47] with next-generation sequencing (NGS) data of miRNAs exhibiting altered expression levels following a similar iLTP stimulation in hippocampal brain slices.[48] This search led to miR153, which targets bases 61-67 of the *Gphn* 3'UTR (Fig. 1A) and is predicted to be downregulated in the hippocampus following iLTP-like stimulation.[48] To verify its downregulation during iLTP, we quantified levels of mature miR153 from cultured hippocampal neurons harvested at multiple time-points following iLTP stimulation using qRT-PCR. This experiment showed that miR153 expression was gradually reduced during iLTP, in comparison with a control miRNA, miR15a (Fig. 1B). This result aligns well with the concurrent increase in gephyrin expression characterized during iLTP.[10]

miR153 silences *Gphn* and controls endogenous gephyrin levels

We next wanted to assess whether miR153 was able to repress *Gphn* mRNA translation via binding to its 3'UTR. To do this, we used reporter plasmids where Firefly luciferase (Luc) was fused to the *Gphn* mRNA 3'UTR, so Luc expression functioned as a readout of *Gphn* translational activity. Luc constructs contained either the wild-type *Gphn* 3'UTR (Luc- $Gphn^{153\text{-}WT}$) or a mutant 3'UTR (Luc-$Gphn^{153\text{-}Mut}$), with mutations in the predicted seed site for miR153 (Fig 1C) and were co-expressed with miR153 in HEK cells (Fig. 1D). Luc activity readings revealed that miR153 overexpression (miR153 OE) decreased translational activity of Luc-$Gphn^{153\text{-}WT}$ by ~45%, compared with control miRNA (miRCon OE). In contrast, translational activity of Luc- $Gphn^{153\text{-}Mut}$ was not impacted by miR153 OE. Notably, Luc-$Gphn^{153\text{-}WT}$ translational activity was significantly lower than that of Luc-$Gphn^{153\text{-}Mut}$ in miR153 OE cells, indicating that the miR153 seed site is required for miR153-mediated translational silencing of gephyrin.

To determine if the miR153 seed site is also important for *Gphn* translational activity in neurons during iLTP, we expressed the Luc-$Gphn^{153\text{-}WT}$ and Luc-$Gphn^{153\text{-}Mut}$ reporters in cultured hippocampal neurons and measured their translational activity (Fig. 1E). Luc-$Gphn^{153\text{-}Mut}$ exhibited higher translational activity than Luc- $Gphn^{153\text{-}WT}$ in control conditions, demonstrating that the miR153 seed site is active and its disruption is sufficient to increase *Gphn* translation in neurons. Furthermore, the translational activity of Luc-$Gphn^{153\text{-}WT}$ was increased following iLTP stimulation, while Luc-$Gphn^{153\text{-}Mut}$ activity was unaltered, suggesting elevated *Gphn* translation during iLTP is controlled by miR153. Together, these data show that miR153 interacts with its

seed site in the *Gphn* 3'UTR to suppress translation in both an *in vitro* reduced system and in hippocampal neurons, revealing a novel mechanism for controlling gephyrin expression. Furthermore, this suppression is relieved in neurons during iLTP, consistent with decreased miR153 neuronal expression following stimulation.

Given that miR153 controls *Gphn* 3'UTR activity, we would expect it to regulate endogenous gephyrin protein expression. To test this idea, we transduced hippocampal neurons with AAVs expressing miRCon or miR153 constructs and used western blotting to measure total gephyrin protein levels (Fig. 1F,G). miR153 OE robustly decreased gephyrin protein levels, with no impact on miR376c targets, $GABA_AR$ $\alpha1$ and $\gamma2$. Furthermore, the expression of $GABA_AR$ subunits $\beta3$ and $\alpha5$ (synaptic and extrasynaptic, respectively) and the AMPA receptor subunit, GluA1, remained unaltered (Fig. S1D,E). We also tested gephyrin protein expression in hippocampal neurons expressing a miR153 inhibitor, which sequesters miR153 thereby reducing expression levels (Fig. 1F,H), and revealed that miR153 inhibition was sufficient to elevate gephyrin protein levels compared to a control inhibitor (miRCon inh.). Similarly, $GABA_AR$ subunits $\alpha1$, $\gamma2$, $\beta3$, $\alpha5$, and GluA1 expression were unaffected by miR153 inhibition (Fig. 1F,H; Fig. S1 D,F), demonstrating that manipulating miR153 levels is sufficient to drive changes in endogenous gephyrin protein expression with little impact on other key synaptic proteins.

miR153 controls gephyrin and $GABA_AR$ synaptic clustering.

Since manipulation of miR153 levels impacted gephyrin translation and total protein levels, we next wanted to determine whether miR153 could control gephyrin expression at synapses. We first assessed gephyrin synaptic clustering in hippocampal cultures overexpressing miR153 or miRCon (GFP reporter, expressed for 48-72 hours), using immunocytochemistry (ICC) with antibodies to gephyrin and the vesicular GABA transporter (VGAT), a marker for GABAergic pre-synaptic terminals (Fig. 2A). For these experiments, sparse transfection of the miRNA constructs allowed us to analyze the impact of miR153 OE specifically in the post-synaptic cell and assess cell-autonomous effects. Confocal imaging and cluster analysis revealed that miR153 OE decreased the area and density of gephyrin and VGAT clusters in neuronal dendrites (Fig. 2B), suggesting that the effects of miR153 on gephyrin expression can alter gephyrin synaptic clustering and impact the number and size of inhibitory synapses. In addition, we observed little effect of miR153 OE on somatic inhibitory synapses (Fig. S2A,B), suggesting potential compartment specificity of miR153 in controlling gephyrin synaptic expression.

Since gephyrin supports GABAergic synaptic structure and function,[16,17,22-30] we reasoned that miR153 may also impact $GABA_AR$ synaptic clusters. To test this hypothesis, we quantified surface $GABA_AR$-$\gamma2$, which serves as a readout of synaptic $GABA_ARs$ ($sGABA_ARs$), and VGAT in neurons transfected with miR153 or miRCon OE constructs (Fig. 2C,D). miR153 OE caused decreased $sGABA_AR$ and VGAT clustering in dendrites, again with no effect on $GABA_ARs$ at inhibitory synapses in the soma (Fig. S2C,D). Furthermore, excitatory synaptic clusters were unaltered in miR153 OE-expressing neurons, indicating that miR153 specifically affects inhibitory connections by manipulating gephyrin expression in the post-synaptic neuron (Fig. S2E,F).

miR153 impacts GABAergic synapse function

Next, we wanted to determine whether miR153-mediated disruption of gephyrin and $GABA_AR$ post-synaptic clustering impacted the efficacy of inhibitory synaptic function. To address this, we used whole-cell voltage-clamp electrophysiology to measure miniature inhibitory synaptic currents (mIPSCs) in cultured neurons overexpressing miR153 or miRCon (Fig. 3A-D). miR153 OE significantly decreased mIPSC frequency, with no effect on mIPSC

amplitude or kinetic properties (Fig. 3A-D; Fig. S3A), indicating a reduction in the total number of functional inhibitory synapses. We also tested whether miR153 OE could impact inhibitory synaptic transmission in an intact circuit by injecting AAVs expressing miR153 or miRCon OE into the hippocampal CA1 region. Acute slices were prepared 2-3 weeks after injection and whole cell recordings of mIPSCs were made from GFP-expressing pyramidal neurons (Fig. 3E-H). As observed in culture, miR153 OE caused a significant decrease in mIPSC frequency compared with miRCon and did not affect mIPSC amplitude or kinetic properties (Fig. 3F; Fig. S3B), again suggesting fewer functional inhibitory synapses in miR153 OE neurons. The lack of impact of miR153 OE on mIPSC amplitude likely reflects the selective effect of miR153 OE on dendritic but not somatic synapses (Fig. S2A-D), which have an augmented contribution to mIPSC measurements made at the soma due to dendritic filtering.

iLTP induces transcriptional repression of miR153

What mechanisms lead to the downregulation of miR153 following iLTP stimulation? We previously found that iLTP stimulation drives transcriptional repression of miR376c, leading to its reduced overall expression which enables increased translation of its targets, *Gabra1* and *Gabrg2*.[10] miR153 levels are also gradually reduced following iLTP stimulation (Fig. 1B), closely mirroring the iLTP-induced decrease in miR376c. Thus, we hypothesized that iLTP stimulation might also induce transcriptional repression of miR153. To test this hypothesis, we used qRT-PCR to assess levels of the miR153 primary transcript (pri-miR153) following iLTP stimulation. Primary miRNAs are the initial transcripts which are processed into mature miRNAs and eventually degraded. Thus, quantification of pri-miRNAs can function as a readout of gene transcription. Pri-miR153 expression was drastically reduced within 10 minutes of iLTP stimulation (Fig. 4A), indicating its rapid transcriptional downregulation. To assess miR153 half-life in neurons under basal conditions, we used actinomycin-D (ActD) to inhibit transcription for up to 90 min and measured mature miR153 levels (Fig. 4B). With ActD treatment, miR153 expression rapidly decreased over time, with levels reduced by ~50% at 20 minutes and ~75% by 90 min. This suggests that miR153 has a relatively high turnover rate in neurons, similar to miR376c.[10] Thus, this short half-life, in combination with its transcriptional repression, likely leads to the gradual reduction in miR153 neuronal expression following iLTP stimulation.

iLTP-induced miR153 transcriptional repression is controlled by calcineurin

During iLTP-induced E-T coupling, NMDARs and LTCCs activate calcineurin (CaN) to facilitate transcriptional repression of miR376c via NFAT and HDAC activity.[10] Since iLTP stimulation also downregulates miR153 through transcriptional repression, we reasoned that a similar E-T coupling pathway could also repress miR153 transcription, to enable coordinated upregulation of gephyrin alongside synaptic $GABA_AR$ subunits. As CaN activation is critical for the downstream E-T signaling to suppress miR376c, we first tested whether iLTP-induced reduction in miR153 also requires CaN activity. We used qRT-PCR to quantify pri-miR153 levels after iLTP stimulation, in the presence or absence of CaN inhibitors cyclosporin A (CsA) or FK506 (Fig. 4C,D). Indeed, blockade of CaN activity completely prevented the reduction in pri-miR153 expression during iLTP (Fig. 4C). Moreover, CaN inhibition also prevented the downregulation of mature miR153 (Fig. 4D), indicating that the reduced expression of miR153 during iLTP is controlled by CaN activation and potentially by a similar E-T coupling pathway as miR376c.

NFATc3 and HDACs control the concurrent transcriptional repression of miR153 and miR376c

During iLTP, transcriptional repression of miR376c is dependent on two NFAT binding sites located at -125 and -109 bp upstream of the precursor miR376c (pre-miR376c) coding region. Our data suggest a model whereby CaN activation promotes NFATc3 translocation to

the nucleus, where it facilitates HDAC-dependent epigenetic repression of miR376c transcription.[10] As with miR376c, we identified a putative NFATc3 binding site -65 bp upstream of the pre-miR153 coding region (Fig. 4E), suggesting that NFATc3 could also modulate miR153 transcription via a similar mechanism. We first determined if the NFATc3 binding site was active by fusing luciferase to the 500 bp sequence upstream of the pre-miR153 coding region (miR153$^{NFAT\text{-}WT}$-Luc; Fig.4E) to provide a readout of miR153 transcriptional activity. When expressed in neurons, miR153$^{NFAT\text{-}WT}$-Luc exhibited an ~5-fold increase in Luc activity compared with an empty luciferase vector, suggesting this region is transcriptionally active (Fig. S4). Following iLTP induction, the activity of miR153$^{NFAT\text{-}WT}$-Luc was reduced by ~60% at 90 min (Fig. 4F) and this reduction was completely prevented by the inclusion of CaN inhibitors, again confirming a significant role for CaN activation in controlling miR153 transcription (Fig. 4G). Crucially, when the NFATc3 binding site in miR153 was mutated (miR153$^{NFAT\text{-}Mut}$-Luc), the iLTP-induced reduction in transcriptional activity was blocked (Fig. 4F). This result suggests that the NFATc3 binding site upstream of the pre-miR153 coding region is active and likely important in regulating miR153 transcription during iLTP.

We also wanted to show that endogenous NFATc3 could repress the transcriptional activity of these upstream regulatory regions of both miR153 and miR376c. To do this, we used shRNA to knockdown NFATc3 (NFAT KD, Fig. S4C) and Luc assays to measure the impact of NFATc3 KD on miR376c and miR153 transcriptional activity (Fig. 4H). Luc measurements revealed that NFAT KD was sufficient to increase transcriptional activity of both miR376c$^{NFAT\text{-}WT}$-Luc and miR153$^{NFAT\text{-}WT}$-Luc in hippocampal neurons, compared to control knockdown (Ctrl KD) and NFATc3 knockdown plus rescue (KD + Rescue) (Fig. 4H). This concurrent increase in the activity of regulatory sequences for both miRNAs establishes a requirement for NFATc3 in reducing the transcription of both miR376c and miR153 during iLTP and suggests a convergent pathway regulating their expression.

Next, we wanted to determine whether HDACs were mediators of miR153 transcriptional repression, as deacetylation of the miR376c promoter region (a mark for gene silencing) is crucial for controlling its transcriptional repression and ultimately $GABA_AR$ expression during iLTP.[10] miR153 expression is regulated by histone acetylation state in other cell types, suggesting that HDACs could indeed impact the levels of miR153.[49] To test if the miR153 regulatory region is de-acetylated during iLTP, we performed chromatin immunoprecipitation (ChIP) assays to quantify the association of acetylated histone H3 within the upstream sequence for miR153 (Fig. 4I). Like miR376c, acetyl-H3 association with miR153 was substantially reduced following iLTP stimulation, a process that was blocked by Ca^{2+} chelation (BAPTA-AM) or CaN inhibition (CsA/FK506). This suggests that miR153 deacetylation could contribute to its transcriptional repression following iLTP stimulation and requires upstream Ca^{2+}-CaN signaling. To confirm the role of HDACs in this signaling pathway, we measured the translational activity of miR376c targets *Gabra1* and *Gabrg2* as well as miR153 target, *Gphn* during iLTP, in the presence or absence of trichostatin A (TSA), which inhibits class I and II HDACs (Fig. 4J). As expected, *Gabra1*, *Gabrg2*, and *Gphn* all exhibited elevated translational activity following iLTP stimulation. However, this was blocked by TSA treatment, demonstrating that HDACs are required for miRNA-mediated increases in inhibitory synaptic gene translation during iLTP.

miR153 downregulation is required for increased GABAergic synaptic clustering during iLTP

Manipulation of miR153 levels alters gephyrin expression and GABAergic transmission, and miR153 levels are reduced following iLTP stimulation. Thus, we predicted that preventing miR153 downregulation during iLTP via miR153 OE would disrupt plasticity-induced changes at inhibitory synapses. To test this prediction, we developed a live-imaging assay to track inhibitory synapse growth and formation in the same cell over time, using the gephyrin intrabody (GPHN-

IB) to label endogenous gephyrin,[50-51] and live antibody labeling of VGAT with VGAT-Oyster^{650}. As we have previously observed in fixed imaging experiments,[10] live imaging revealed a steady increase in gephyrin and VGAT cluster intensity and density in the 90 min following iLTP stimulation, showing an increase in the number and size of inhibitory synapses during iLTP (Fig. S5A-C). Importantly, application of the translational inhibitor cycloheximide (CHX), blocked the maintenance of this increased clustering at 90 min post-stimulation, recapitulating our findings using fixed-cell confocal imaging.[10] We then used this approach to determine how preventing miR153 downregulation would impact iLTP-induced increases in inhibitory size and density (Fig. 5A-C; Fig. S5D). We sparsely expressed GPHN-IB and fluorescently tagged miRCon or miR153 OE constructs (~72 hr), live labeled with VGAT-Oyster^{650}, and imaged neuronal dendrites in sham or iLTP conditions. As expected, gephyrin synaptic cluster intensity increased steadily in miRCon OE neurons treated with iLTP conditions compared with sham-stimulated controls. In contrast, miR153 OE-expressing neurons exhibited no increase in inhibitory synaptic clustering over time following stimulation, suggesting that preventing reduced miR153 expression during iLTP stimulation is sufficient to disrupt persistent iLTP-dependent increases in synaptic clustering and density.

As miR153 OE prevented increased synaptic clustering of gephyrin and VGAT following iLTP stimulation, we then examined whether this also impacts the iLTP-induced upregulation of $GABA_AR$ clusters at synapses (Fig. 5D-E). ICC experiments using neurons expressing miRCon or miR153 and confocal imaging revealed an expected increase in $GABA_AR$ and VGAT clusters in miRCon OE neurons at 90 min following iLTP, while this elevated synaptic clustering of $GABA_ARs$/VGAT was blocked by miR153 OE. These data indicate that the reduction in miR153 expression following iLTP stimulation is a crucial mechanism regulating GABAergic synapse clustering during persistent iLTP.

CaN signaling orchestrates sustained inhibitory synapse upregulation during iLTP

Our data show that following iLTP stimulation, CaN signaling controls downstream transcriptional repression of both miR376c and miR153.[10] However, it is unclear if this signaling ultimately leads to sustained increases in inhibitory synapse size and density during iLTP. To first assess whether CaN activity is required for *Gphn* translation, we performed Luc reporter assays to measure the translational activity of the *Gphn* 3'UTR during iLTP (Fig. 6A). Inclusion of BAPTA or CsA/FK506 prevented the iLTP-induced increase in translational activity of *Gphn* 3'UTR, implicating Ca^{2+}-CaN activity in the pathway driving gephyrin translation during iLTP. Furthermore, analysis of total gephyrin levels following stimulation revealed that Ca^{2+}-chelation or CaN inhibition could also robustly block the increase in gephyrin protein expression during iLTP (Fig. 6B,C). Given that CaN mediates the upregulation of $GABA_AR$ translation and protein expression during iLTP,[10] we then wanted to assess whether CaN acts as the primary signal for the persistent increase in inhibitory synapse size and number following iLTP stimulation. Again, we performed live-imaging of gephyrin and VGAT clusters over time following iLTP stimulation. Inhibition of CaN during iLTP blocked increased synaptic clustering of gephyrin, and the growth and formation of GABAergic synapses compared with control conditions (Fig. 6D-F; Fig. S6A). These results mirrored what we observed in miR153 OE neurons (Fig. 5), demonstrating that preventing reduced miR153 expression during iLTP through its overexpression or via disruption of Ca^{2+}-CaN signaling is sufficient to block elevated inhibitory synaptic upregulation during iLTP. Altogether, these results characterize key players for altering miR153 expression following iLTP stimulation and establish a shared signaling pathway which leverages miR376c and miR153 to control changes in gene expression for multiple transcripts during iLTP.

DISCUSSION

In neurons, proteins are continuously synthesized and degraded to shape the synaptic proteome.[7,13] miRNAs are crucial regulators of synaptic protein production, and therefore can significantly impact the protein composition at synapses, modifying synaptic strength and controlling various types of synaptic plasticity.[52] In previous work, we showed that gephyrin and $GABA_AR$ expression at synapses increased and was maintained over time following iLTP stimulation, a process dependent on translation.[10] Although we found that miR376c controlled synaptic $GABA_AR$ subunit translation during this process, it still remained unclear what post-transcriptional mechanisms regulated the upregulation of the crucial scaffold, gephyrin, during iLTP. Here, we now show that a different miRNA, miR153, controls the synthesis of gephyrin following iLTP stimulation. This finding reveals a complementary mechanism to upregulate gephyrin, alongside miR376c-controlled translation of synaptic $GABA_ARs$, and hints that numerous concurrent post-transcriptional mechanisms may coordinate *de novo* synthesis of the myriad proteins required to strengthen synaptic inhibition during plasticity.

miRNA-dependent post-transcriptional regulation of gephyrin translation

Given the central role of gephyrin in mediating GABAergic synaptic transmission,[17,22-30] it is surprising how little is known about mechanisms controlling its translation. Here, we discovered a mechanism whereby miR153 represses the translation of gephyrin in neurons under basal conditions; this repression is relieved following iLTP stimulation, allowing for gephyrin *de novo* synthesis. It is highly likely that miR153 is not the only factor which regulates gephyrin expression at the post-transcriptional level. Screening of the rodent *Gphn* 3'UTR predicted seed sites for eight additional miRNAs, indicating that other non-coding RNAs may also control gephyrin synthesis. In addition, multiple RNA-binding proteins (RBPs), including Nova, Staufen2, Rbfox1-3, and Pumilio2 (Pum2) can target *Gphn* mRNA,[53-57] indicating a broad range of potential mechanisms to control gephyrin translation. Recent work confirmed that gephyrin is a Pum2 target,[56] and identified Pum2 as a potential regulator of post-transcriptional gephyrin expression in the cerebral cortex.[58] Further, *Gphn* mRNA can undergo extensive splicing,[59-61] which recently was shown to govern its postsynaptic clustering properties at different types of inhibitory synapses and contributing to synaptic diversity.[17,62-65] It is likely that many of these mechanisms are brain region or cell-type specific, and possibly active during specific times in development or in different types of plasticity, thereby enabling precise control of gephyrin expression in diverse scenarios.

Overexpression of miR153 substantially reduced gephyrin and $GABA_AR$ synaptic clustering in dendrites, which correlated with reduced synaptic inhibition observed in our electrophysiology experiments. Analysis revealed a substantially reduced mIPSC frequency, but no change in mIPSC amplitude, both in hippocampal culture and CA1 acute slices. This result indicates a loss of functional synapses, which could be caused by the reduction of gephyrin and $GABA_AR$ synaptic clustering, if their expression decreased such that receptor activation by a single vesicle falls below the detection limit of our measurements. Furthermore, our imaging results suggest that somatic GABAergic synapses are not impacted by miR153 overexpression. Thus, changes in the amplitude of mIPSC events originating in the dendrites will likely be masked by the unaltered mIPSCs recorded in the soma, which have an outsized contribution to mIPSC measurements due to dendritic filtering of synaptic responses occurring remotely in dendrites.[10,66]

The specific mechanism which enables miR153 to exclusively impact dendritic GABAergic synaptic clustering remains unclear. Some miRNAs are enriched in neuronal dendrites and can even undergo local processing into mature miRNA transcripts in response to activity, enabling rapid, compartment-specific alterations in expression of their targets during

plasticity.[67-68] An alternative mechanism may rely on subcellular localization of the target transcript, driven by multiple 3'UTR variants which are differentially expressed in distinct neuronal compartments.[10,69] However, *Gphn* mRNA does not appear to have variants with alternative 3'UTRs,[69] suggesting that the compartment-specific effect of miR153 expression on gephyrin and $GABA_A$Rs is likely due to an alternative mechanism, such as coordination with specifically-localized RBPs or the localization of miR153 itself. Given that miR153 expression selectively affects dendritic inhibitory synapses, it is tempting to speculate that local translation of gephyrin in dendrites supports changes in expression during iLTP, as we observed with $GABA_A$R mRNAs,[10] and has been shown for many excitatory synaptic transcripts during plasticity.[11,69-72] Future work will be essential to identify the mechanism underlying the compartment-specific impact of miR153 and whether dendritic gephyrin translation is involved.

Impact of miR153 on cellular processes and neural function

Like most miRNAs, miR153 is predicted to target numerous genes besides *Gphn*. Notably, miR153 has been shown to suppress translation of mRNAs encoding proteins involved in presynaptic active zone scaffolding and vesicle trafficking and release, including VAMP2 and SNAP25.[73] As a result, it is possible that overexpression of miR153 may impact neurotransmitter release. For this reason, when testing how miR153 OE affects GABAergic synapse structure and function, we used sparse transfection, allowing us to examine the cell-autonomous impact of miR153 OE on the postsynaptic neuron without interfering with presynaptic neurotransmitter release. Because of its impact on presynaptic function and plasticity, miR153 is implicated in broad-reaching functions like contextual fear learning, neuronal precursor proliferation and neurogenesis, and hippocampal-dependent cognitive tasks.[73-76] Furthermore, dysregulated miR153 expression has been implicated in Alzheimer's disease and autism spectrum disorders,[74-77] both of which are linked to disrupted synaptic inhibition.[78-83] Our findings suggest that the role of miR153 in controlling inhibitory synaptic function and plasticity may contribute to these pathologies.

E-T coupling coordinates transcriptional repression of miRNAs during iLTP

Our results show that miR153 expression is downregulated following iLTP stimulation via an E-T coupling pathway involving CaN, NFAT, and HDACs. This pathway mirrors the signaling that is required to downregulate miR376c during iLTP and suggests that the same signaling components control the expression of both miR153 and miR376c. Like miR376c, iLTP-induced suppression of miR153 levels is likely through rapid transcriptional repression, and the subsequent degradation of the mature miRNA. This is supported by our ActD experiments which show that upon transcriptional inhibition, miR153 expression levels are rapidly reduced, indicating that miR153 has a short half-life, which is common in neural tissues like the brain and retina.[84-86]

Put together with our previous work,[10] our present findings suggest a model whereby iLTP stimulation activates CaN, which can drive the rapid translocation of NFATc3 into the nucleus. NFAT binds to regulatory sites upstream of the pre-miRNA coding sequences of miR153 and miR376c and promotes transcriptional repression through the likely recruitment of HDACs. Although the canonical promoter sequence for miR153 is located further upstream from this region,[73] we hypothesize that the sequence we used in our experiments functions as an alternative promoter or, perhaps more likely, a crucial regulatory region to modulate miR153 expression. Indeed, our data suggest that NFATc3 may recruit HDACs to alter the acetylation state of these upstream regulatory regions thus coordinately downregulating miR153 and miR376c transcription. This non-canonical role of NFATc3 in repressing miRNA transcription through an epigenetic mechanism is poorly characterized and will require further study to assess the extent of its impact in synaptic plasticity.

We have found that a single NMDA stimulation leads to dynamic alterations in the expression of two miRNAs, which target different synaptic genes in the same functional pathway. This coordinated control of miRNAs is also observed for modulation of glutamatergic synapse strength during synaptic plasticity. For instance, during excitatory LTD, miR135 and miR191 control expression of their targets (complexins and Tmod2) to coordinate the shrinkage of dendritic spines.[48] Conversely, following excitatory LTP stimulation, miR26a and miR384-5p work in concert to control the maintenance of spine enlargement, a hallmark for LTP.[87] Given that there are many other proteins which support inhibitory synaptic function beyond gephyrin and $GABA_A$Rs, we suspect that iLTP stimulation likely drives changes in expression for other genes involved in synaptic inhibition. It is possible that the signaling pathway we have identified here leverages an even broader miRNA network to control expression of these transcripts. Future work is aimed at identifying other genes whose translation is important for inhibitory synaptic plasticity, and whether this translation is controlled by a similar pathway. Characterizing these mechanisms is crucial to our understanding of how neurons control synaptic inhibition to maintain E/I balance and identifying potential therapeutic targets when that balance is disrupted.

Figures

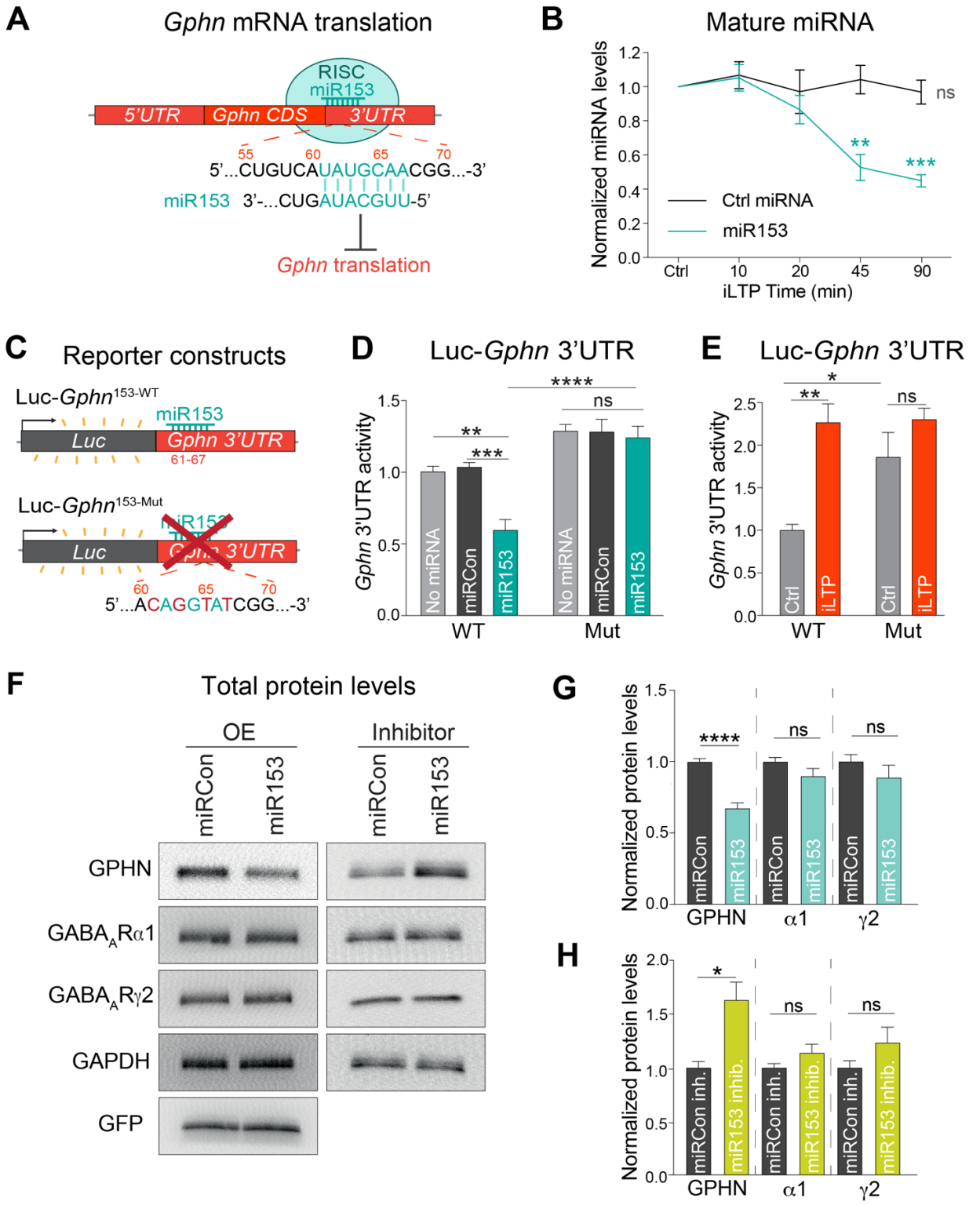

Figure 1. miR153 is downregulated during iLTP and controls endogenous gephyrin expression

(A) Schematic of RNA-Induced Silencing Complex (RISC) and miR153 interaction with the seed site in *Gphn* 3'UTR, which is predicted to suppress translation of this mRNA.

(B) qRT-PCR of miR153 and miR15a (Ctrl miRNA) expression in cultured hippocampal neurons harvested at different time-points following iLTP stimulation. miRNA levels were normalized to U6. n = 4.
(C) Schematic of the Luc-*Gphn* luciferase reporters. miR153 seed site is mutated in Luc-*Gphn*$^{153\text{-Mut}}$.
(D) Quantification of Luc-*Gphn* activities in HEK293T cells co-expressing control miRNA (miRCon), miR153, or no miRNA. Firefly was normalized to Renilla, and the data quantified as relative change in normalized Luc activity. n = 5.
(E) Quantification of Luc-*Gphn* activities in hippocampal neurons under control conditions (Ctrl) or 90 min post-iLTP stimulation. n = 5.
(F) Western blots of gephyrin (GPHN), $GABA_AR$ subunits α1 and γ2, GAPDH, and GFP protein levels in neurons overexpressing miRCon or miR153 (left), and miRCon inhibitor or miR153 inhibitor (right). miRNA overexpression (OE) constructs contain a GFP reporter.
(G) Quantification of GPHN, α1, and γ2 levels in miRCon or miR153 OE neurons. Protein levels were normalized to GAPDH, and the data quantified as relative change in normalized protein expression. n = 5.
(H) Quantification of GPHN, α1, and γ2 in neurons expressing miRCon or miR153 inhibitors. n = 4.

All values represent mean ± SEM. *p<0.05 and **p<0.01, ***p<0.005, ****p<0.0001; one-sample t-test (B), two-way ANOVA with Tukey's multiple comparisons post-hoc test (D,E), and Mann-Whitney test (G,H).

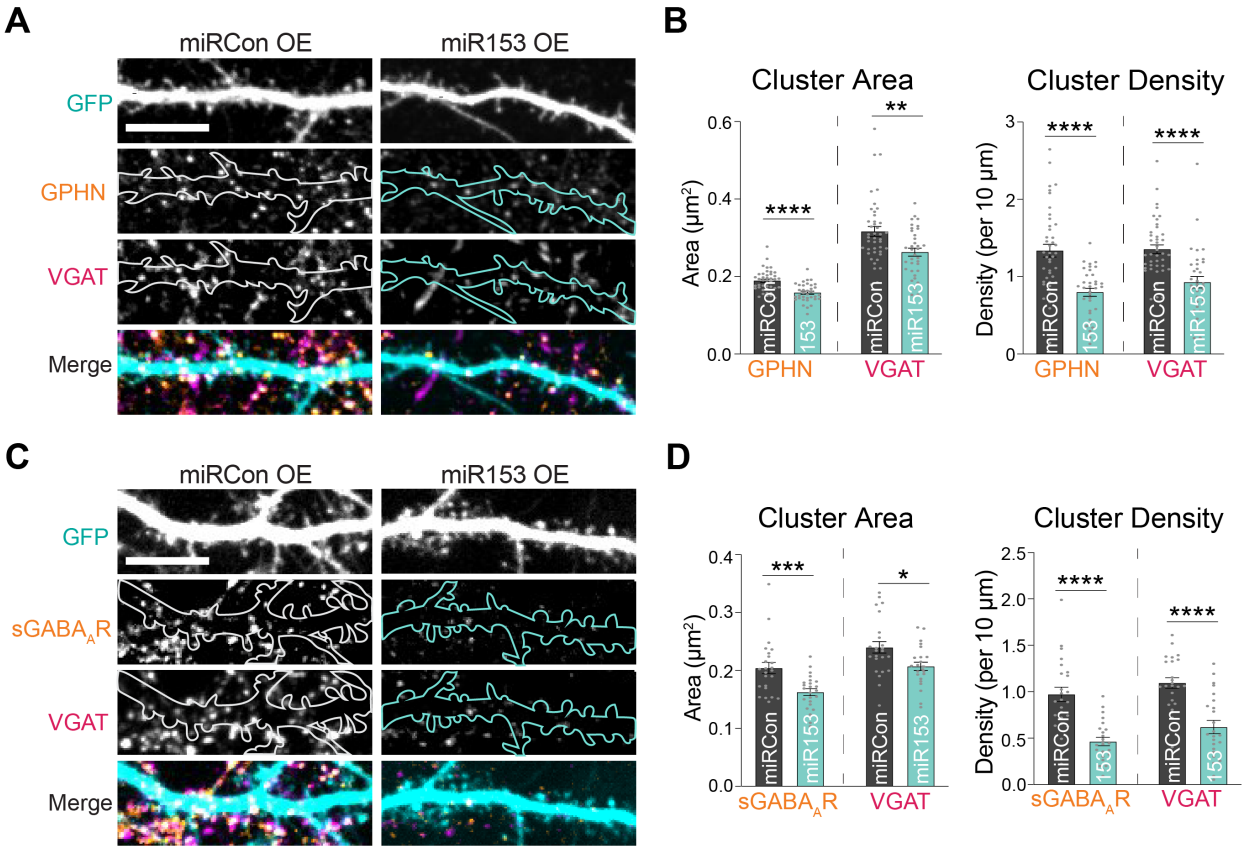

Figure 2. miR153 overexpression disrupts gephyrin and GABA$_A$R synaptic clustering

(A) Representative dendritic segments of miRCon or miR153 OE-expressing neurons labeled with antibodies to gephyrin (GPHN) and VGAT. Scale bar, 10 µm.

(B) Quantification of GPHN and VGAT cluster area (left) and cluster density (right) in neurons from (A). n = 35-42 neurons per condition.

(C) Representative dendritic segments of miRCon or miR153 OE-expressing neurons labeled with antibodies to surface GABA$_A$R subunit γ2 (sGABA$_A$R) and VGAT. Scale bar, 10 µm.

(D) Quantification of sGABA$_A$R and VGAT cluster area (left) and cluster density (right) in neurons from (C). n = 24 neurons per condition.

All values represent mean ± SEM. *p<0.05 and **p<0.01, ***p<0.005, ****p<0.0001; Mann-Whitney test.

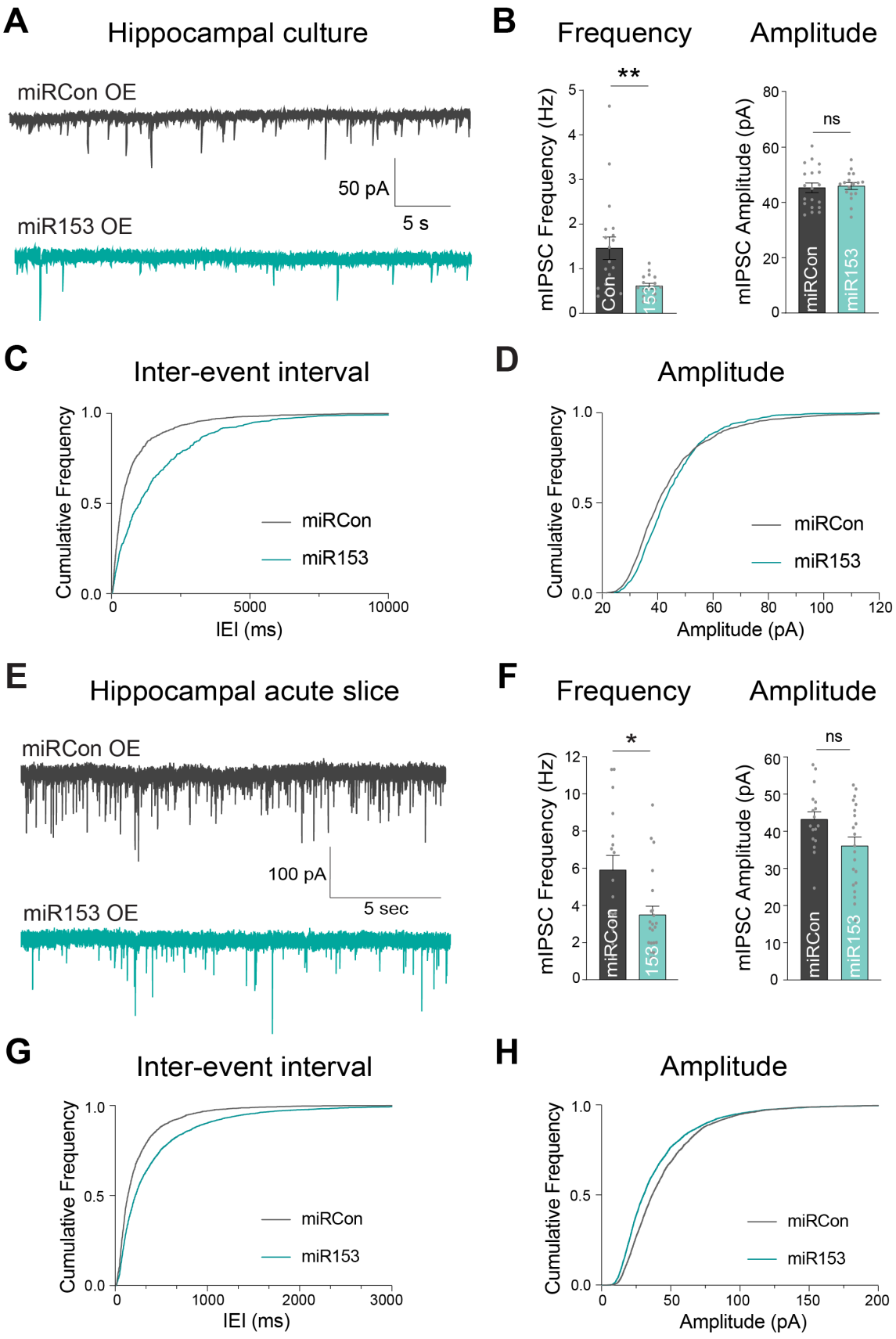

Figure 3. miR153 overexpression impacts GABAergic synaptic transmission

(A) Representative mIPSC current traces from miRCon and miR153 OE-expressing neurons in hippocampal culture.
(B) Quantification of mIPSC frequency (left) and amplitude (right) from miRCon and miR153 OE-expressing neurons. n = 17-19 neurons per condition.
(C) Cumulative frequency distribution of mIPSC inter-event intervals (IEI) for events in miRCon and miR153 OE-expressing neurons.
(D) Cumulative frequency distribution of mIPSC amplitude for events in miRCon and miR153 OE-expressing neurons.
(E) Representative traces recorded from miRCon and miR153 OE-expressing neurons in acute hippocampal slices.
(F) Quantification of mIPSC frequency (left) and amplitude (right) from miRCon and miR153 OE-expressing neurons. n = 17-22 neurons per condition.
(G) Cumulative frequency distribution of mIPSC IEI for events in miRCon and miR153 OE-expressing neurons.
(H) Cumulative frequency distribution of mIPSC amplitude for events in miRCon and miR153 OE-expressing neurons.

All values represent mean ± SEM. *p<0.05 and **p<0.01, ***p<0.005, ****p<0.0001; Mann-Whitney test.

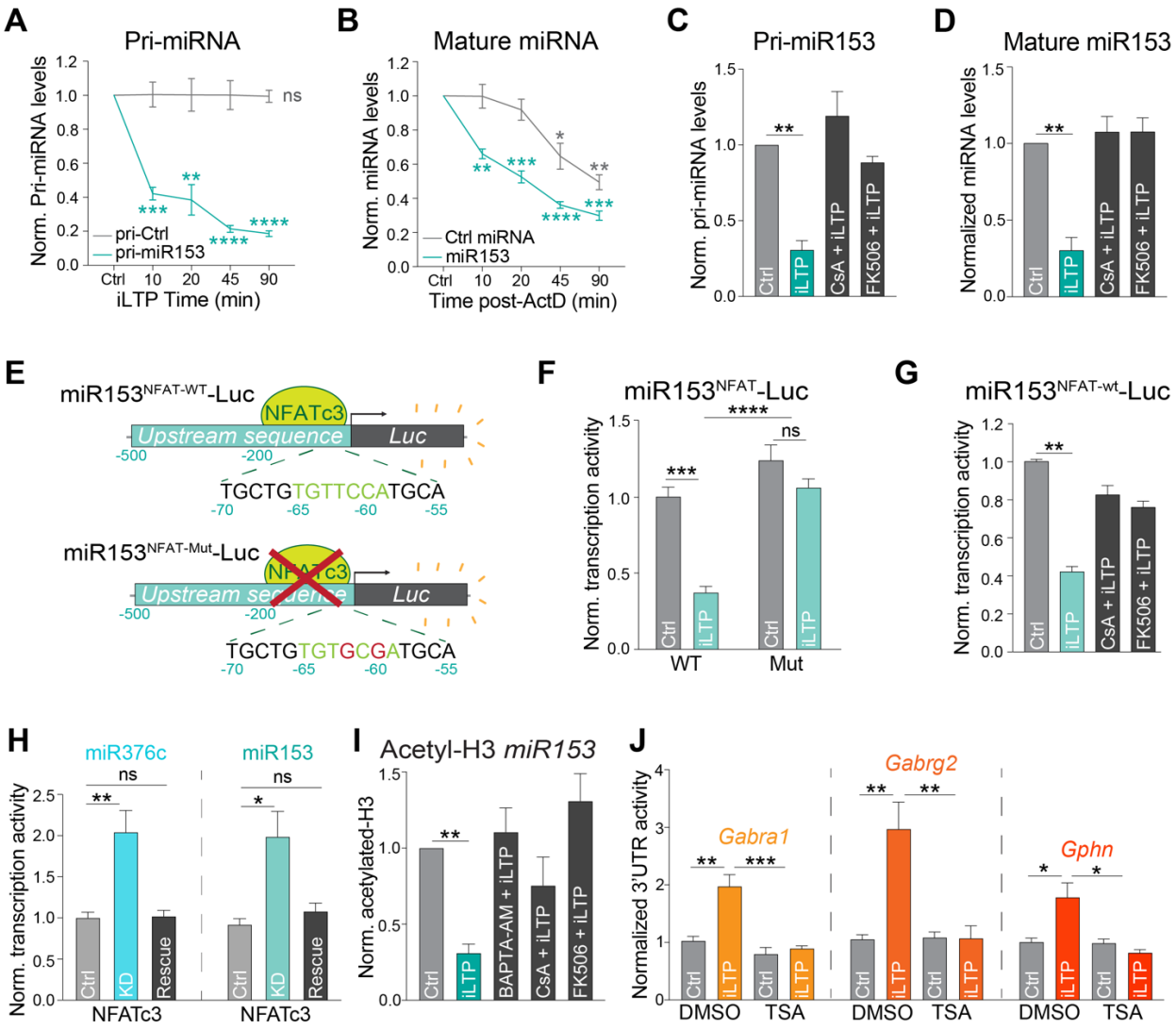

Figure 4. miR153 and miR376c transcriptional repression are controlled by a common CaN-NFAT signaling pathway during iLTP

(A) qRT-PCR of primary miR153 transcript (pri-miR153) and pri-miR410 (pri-Ctrl) expression in neurons harvested at increasing time-points following iLTP stimulation. pri-miRNA levels were normalized to U6 and quantified as fold change from Ctrl condition. n = 4.

(B) qRT-PCR of mature miR153 and miR410 (Ctrl miRNA) expression in neurons harvested at increasing time-points following treatment with actinomycin-D (ActD). miRNA levels normalized to U6 and quantified as fold change from Ctrl condition. n = 4.

(C) qRT-PCR of pri-miR153 expression in hippocampal neurons following control treatment (Ctrl) or 90 min post-iLTP stimulation in the presence or absence of CaN inhibitors cyclosporin A (CsA) and FK506. Quantified as fold change in pri-miR153 levels from Ctrl condition. n=4

(D) qRT-PCR of mature miR153 expression in Ctrl and iLTP-90 neurons in the presence or absence of CsA and FK506. Quantified as miR153 fold change from Ctrl condition. n=5

(E) Schematic of the miR153-Luc luciferase reporters. Predicted NFAT binding site is mutated in miR153$^{NFAT-Mut}$-Luc.

(F) Quantification of miR153-Luc activities in neurons under control conditions (Ctrl) or 90 min post-iLTP stimulation. Firefly was normalized to Renilla, and the data quantified as relative change in normalized Luc activity with error-corrected control values. n = 4.

(G) Quantification of miR153-Luc activities in Ctrl and iLTP-90 neurons in the presence or absence of CsA and FK506. n = 4.
(H) Quantification of miR376c-Luc and miR153-Luc activities in Ctrl, NFATc3 knockdown (KD) and NFATc3 KD + rescue (Rescue) neurons. n = 7.
(I) qPCR readout of acetyl-histone H3 chromatin immunoprecipitation (ChIP) from neurons to show acetylation status of the miR153 promoter in Ctrl and iLTP-90 conditions in the presence or absence BAPTA-AM, CsA, and FK506. n = 4.
(J) Quantification of miR153-Luc activities in Ctrl and iLTP-90 neurons in the presence or absence of CsA and FK506. Quantified as fold change in miR153-Luc activity from Ctrl condition. n = 4.
(K) Quantification of Luc-*Gabra1*, Luc-*Gabrg2*, and Luc-*Gphn* activities in Ctrl and iLTP-90 neurons in the presence or absence of HDAC inhibitor trichostatin-A (TSA). n = 4.

All values represent mean ± SEM. *p<0.05 and **p<0.01, ***p<0.005, ****p<0.0001; one-sample t-test (A-D,I), two-way ANOVA with Tukey's multiple comparisons post-hoc test (F,J), and Kruskal-Wallis with Dunn's multiple comparisons post-hoc test (G,H).

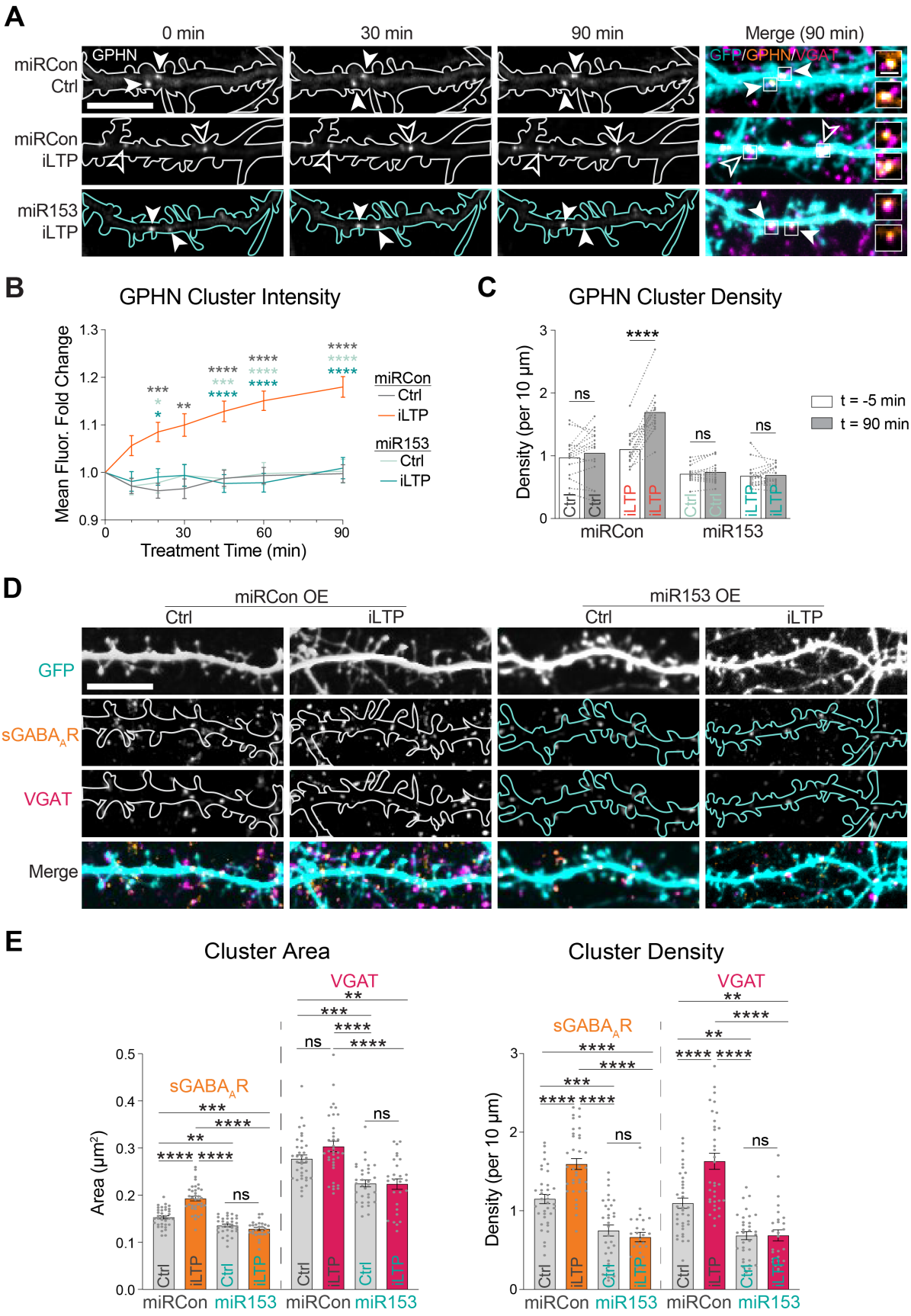

Figure 5. miR153 overexpression prevents increased GABAergic synaptic clustering during iLTP

(A) Representative dendritic segments of miRCon or miR153 OE-expressing neurons over time in control and iLTP conditions. Neurons co-expressed the gephyrin intrabody (GPHN IB, arrowheads) and labeled live with VGAT Oyster^{650}. Puncta are labeled with filled arrowheads when the fluorescence is unchanged and open arrowheads when fluorescence increases over time. Boxes indicate the fluorescent puncta enlarged in the merged images (dendrite scale bar, 10 μm; synapse scale bar, 2 μm).

(B) Quantification of fold change in GPHN puncta fluorescence intensity over time following treatment in neurons from (A). n = 15 neurons per condition, 10 puncta per neuron.

(C) Paired measurements of GPHN cluster density in dendrites prior to (-5 min) and 90 min following treatment. n = 15 neurons per condition.

(D) Representative dendritic segments of miRCon or miR153 OE-expressing neurons labeled with antibodies to surface $GABA_AR$ γ2 subunit ($sGABA_AR$) and VGAT following control treatment or 90 min post-iLTP stimulation. Scale bar, 10 μm

(E) Quantification of $sGABA_AR$ and VGAT cluster area (left) and density (right) in neurons from (D). n = 27-36 neurons per condition.

All values represent mean ± SEM. *p<0.05 and **p<0.01, ***p<0.005, ****p<0.0001; RM two-way ANOVA with Geisser-Greenhouse correction (B) and Šidák's multiple comparisons post-hoc test (B,C) and ordinary two-way ANOVA with Tukey's multiple comparisons post-hoc test (E).

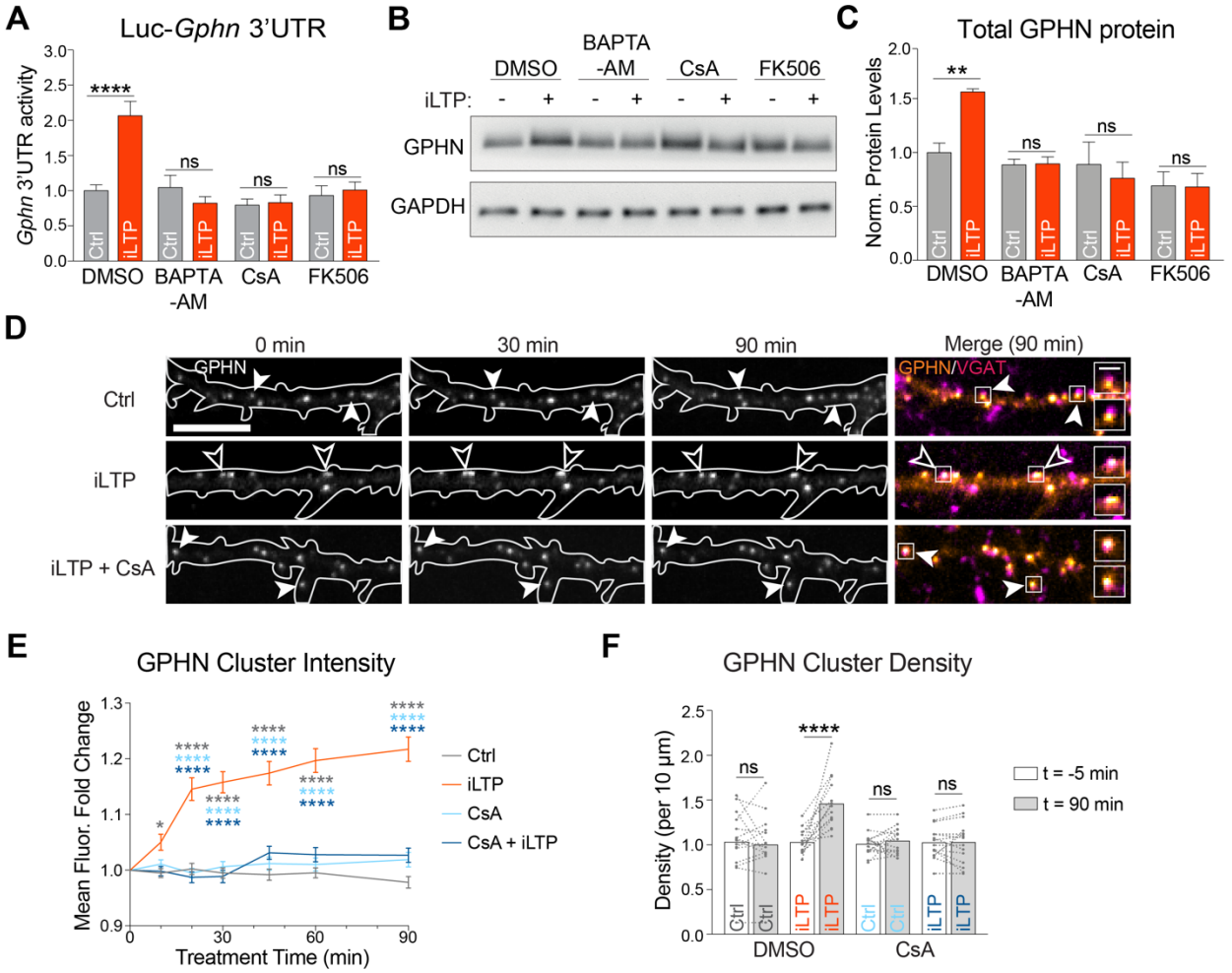

Figure 6. Calcium and calcineurin signaling are required for increased gephyrin translation and synaptic clustering during iLTP

(A) Graph of Luc-*Gphn* activities in Ctrl or iLTP-90 neurons in the presence or absence of BAPTA, CsA, and FK506. Firefly was normalized to Renilla, and the data quantified as relative change in normalized Luc activity. n = 5.

(B) Western blots of GPHN and GAPDH protein levels in Ctrl and iLTP-90 neurons in the presence or absence of BAPTA, CsA, and FK506.

(C) Quantification of GPHN from western blots in (B). Protein levels were normalized to GAPDH, and the data quantified as relative change in normalized protein expression. n = 6.

(D) Representative dendritic segments of neurons expressing GPHN IB and labeled with an antibody to VGAT, imaged over time in control and iLTP conditions in the presence or absence of CsA. Puncta are labeled with filled arrowheads when the fluorescence is unchanged and open arrowheads when fluorescence increases over time. Boxes indicate the fluorescent puncta enlarged in the merged images (dendrite scale bar, 10 µm; synapse scale bar, 2 µm).

(E) Quantification of fold change in GPHN puncta fluorescence intensity in neurons over time following treatment, as shown in (D). n = 15 neurons per condition, 10 puncta per neuron.

(F) Paired measurements of GPHN cluster density in dendrites prior to (-5 min) and 90 min following treatment. n = 15 neurons per condition.

All values represent mean ± SEM. *p<0.05 and **p<0.01, ***p<0.005, ****p<0.0001; ordinary (A,C) or RM (E,F) two-way ANOVA with Geisser-Greenhouse correction (E) and Šidák's multiple comparisons post-hoc test.

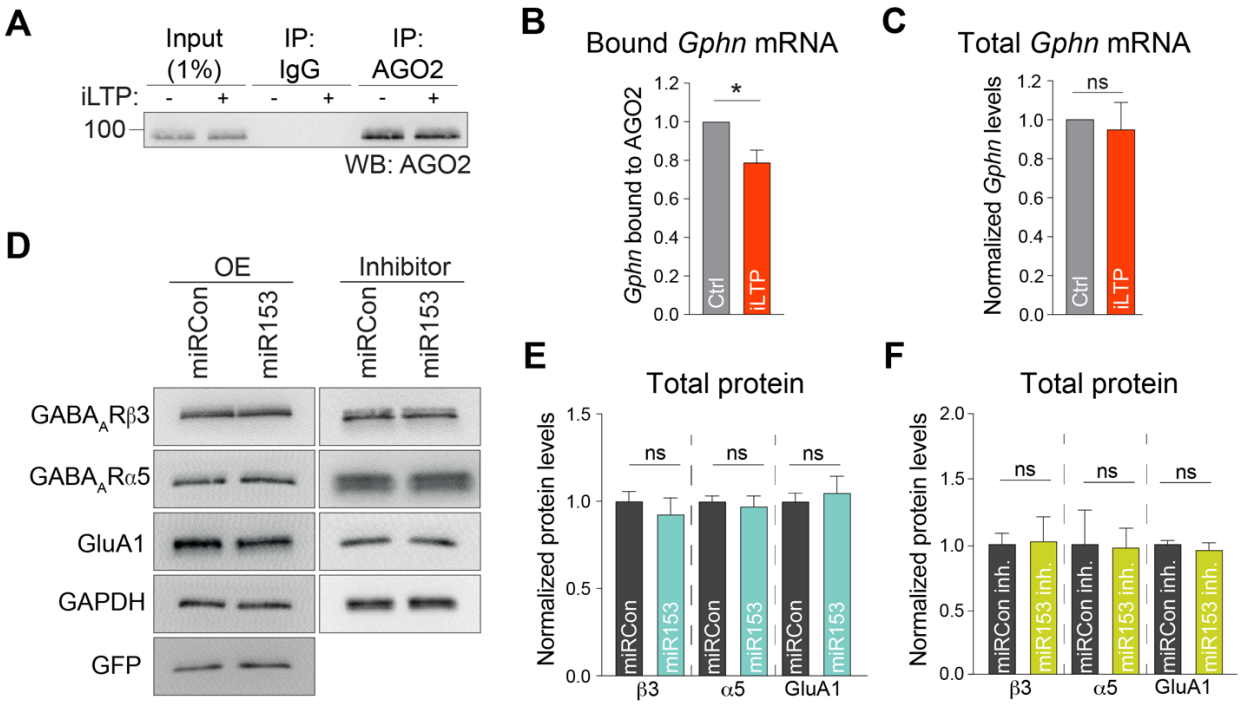

Figure S1. Supplement to Figure 1

(A) Western blot (WB) of AGO2 immunoprecipitated from neurons following control treatment (Ctrl) or 90 min post-iLTP stimulation (iLTP).

(B) qRT-PCR of *Gphn* mRNA bound to AGO2 in neurons from (A). AGO2-bound *Gphn* was normalized to total *Gphn* mRNA expression, and fold change from Ctrl was quantified for each condition. n = 4.

(C) qRT-PCR of total *Gphn* mRNA levels in Ctrl and iLTP-90 neurons. *Gphn* mRNA levels were normalized to U6 expression, and fold change from Ctrl was quantified for each condition. n = 3.

(D) Western blots of GABA$_A$R subunits β3 (synaptic) and α5 (extrasynaptic), AMPAR subunit GluA1, GAPDH, and GFP protein levels in neuron overexpressing miRCon or miR153 (left), and miRCon inhibitor or miR153 inhibitor (right). miRNA overexpression (OE) constructs contain a GFP reporter.

(E) Quantification of β3, α5, and GluA1 in miRCon or miR153 OE neurons. Protein levels were normalized to GAPDH, and the data quantified as relative change in normalized protein expression. n = 5.

(F) Quantification of β3, α5, and GluA1 in neurons expressing miRCon or miR153 inhibitors. n = 4.

All values represent mean ± SEM. *p<0.05 and **p<0.01, ***p<0.005, ****p<0.0001; one-sample t-test (B), Wilcoxon signed rank test (C), and Mann-Whitney test (E,F).

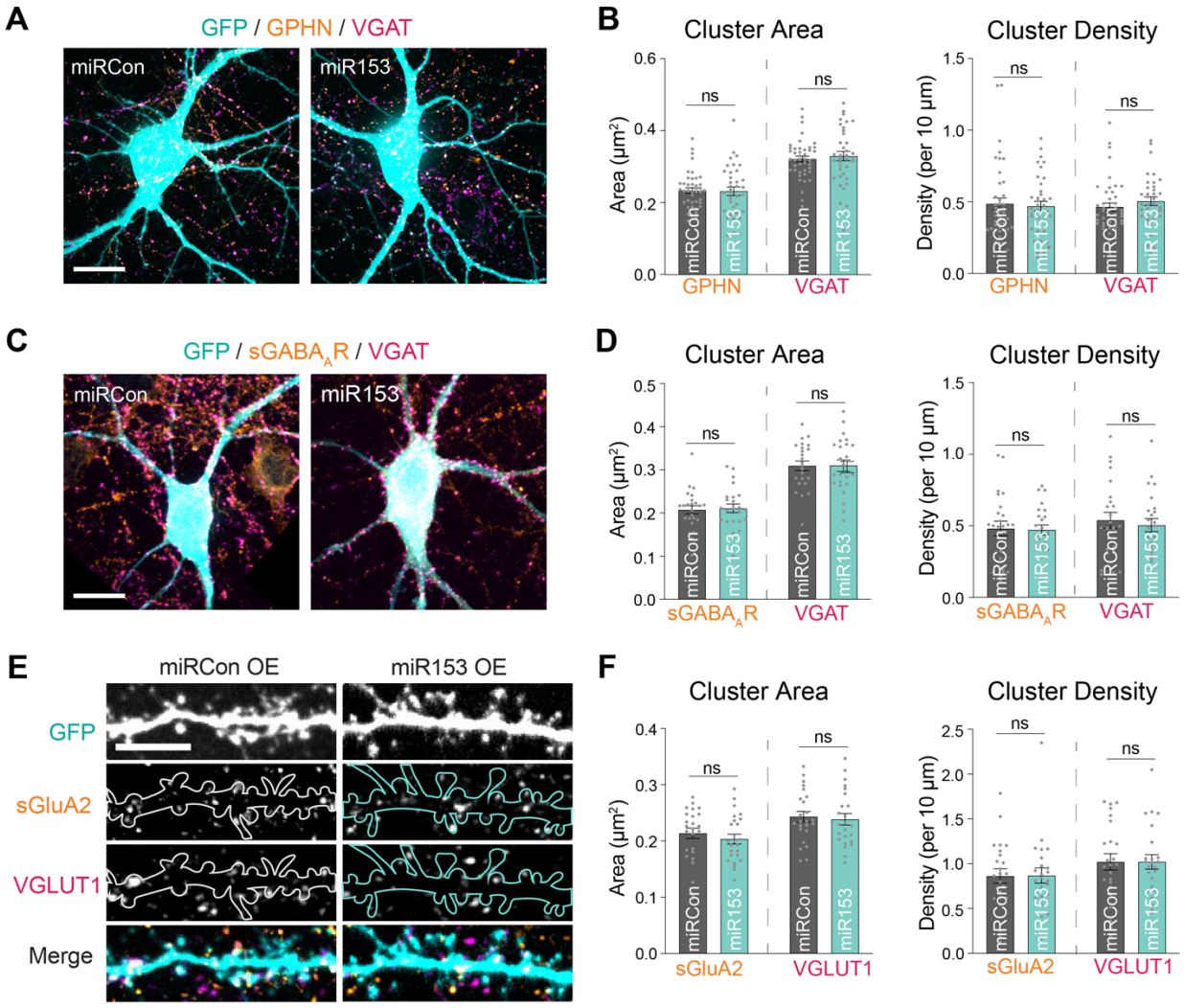

Figure S2. Supplement to Figure 2

(A) Representative somata of miRCon or miR153 OE-expressing neurons labeled with antibodies to GPHN and VGAT. Scale bar, 80 µm.

(B) Quantification of GPHN and VGAT cluster area (left) and cluster density (right) in neurons from (A). n = 37-43 neurons per condition.

(C) Representative somata of miRCon or miR153 OE-expressing neurons labeled with antibodies to surface $GABA_AR$ γ2 subunit ($sGABA_AR$) and VGAT. Scale bar, 80 µm.

(D) Quantification of $sGABA_AR$ and VGAT cluster area (left) and cluster density (right) in neurons as shown in (C). n = 24 neurons in each condition.

(E) Representative dendritic segments of miRCon or miR153 OE neurons labeled with antibodies to surface AMPAR subunit GluA2 (sGluA2) and VGLUT1.

Scale bar, 80 µm.

(F) Quantification of surface GluA2 and VGLUT1 cluster area (left) and cluster density (right) in neurons from (C). n = 24 neurons per condition.

All values represent mean ± SEM. *p<0.05 and **p<0.01, ***p<0.005, ****p<0.0001; Mann-Whitney test.

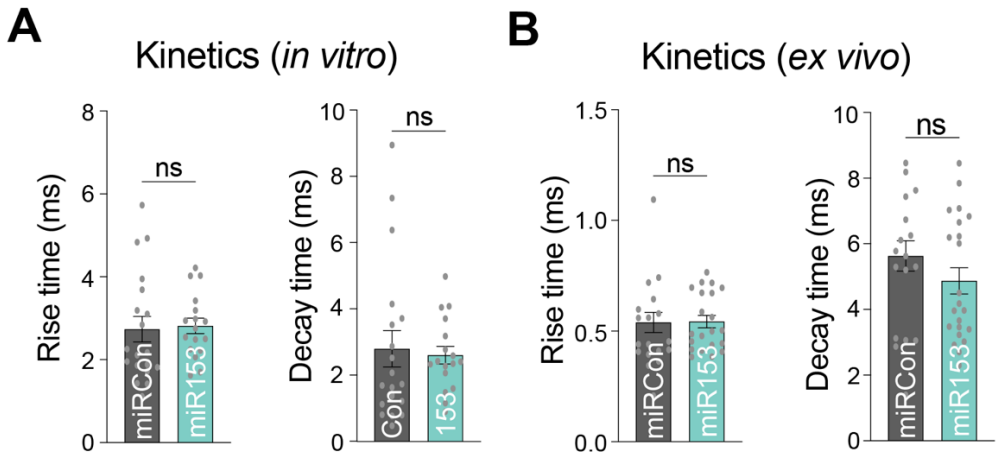

Figure S3. Supplement to Figure 3

(A) Quantification of mIPSC rise time (left) and decay time (right) from miRCon and miR153 OE-expressing neurons in culture. n = 17-19 neurons per condition.

(B) Quantification of mIPSC rise time (left) and decay time (right) from miRCon and miR153 OE-expressing neurons in slice. n = 17-21 neurons per condition.

All values represent mean ± SEM. *p<0.05 and **p<0.01, ***p<0.005, ****p<0.0001; Mann-Whitney test.

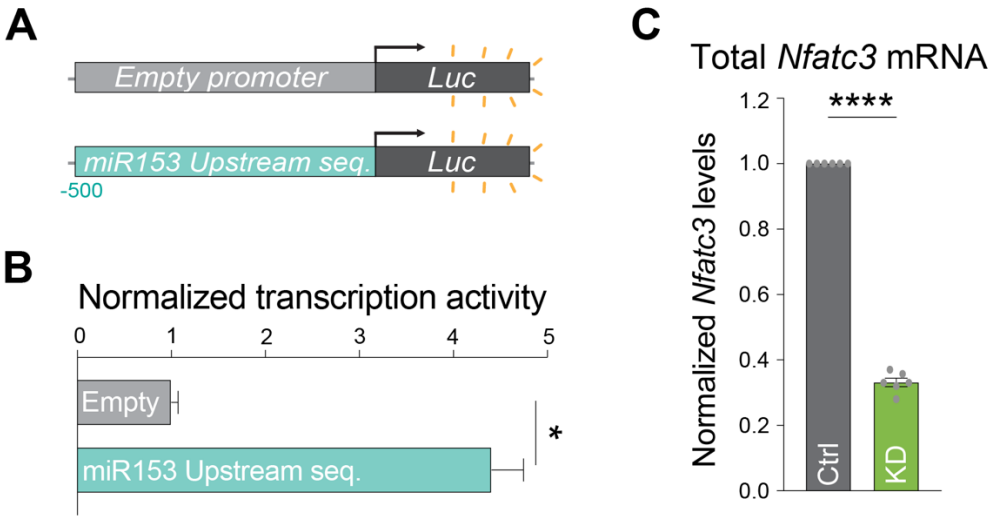

Figure S4. Supplement to Figure 4

(A) Schematic of the Empty-Luc (no promoter) and miR153^{-500}-Luc luciferase reporters, designed to test transcriptional activity of the sequence 500 bp upstream of miR153.

(B) Quantification of Luc activities in neurons expressing reporters containing no promoter (Empty) or the sequence upstream of pri-miR153 coding region (miR153 Upstream seq.). Firefly was normalized to Renilla, and the data quantified as relative change in normalized Luc activity with error-corrected control values. n = 4.

(C) qRT-PCR of total *Nfatc3* mRNA levels in Ctrl and NFATc3 knockdown (NFAT KD) neurons. *Nfatc3* mRNA levels normalized to *Gapdh* mRNA expression, and fold change from Ctrl was quantified for each condition. n = 6.

All values represent mean ± SEM. *p<0.05 and **p<0.01, ***p<0.005, ****p<0.0001; Mann-Whitney test (B) and one-sample t-test (C).

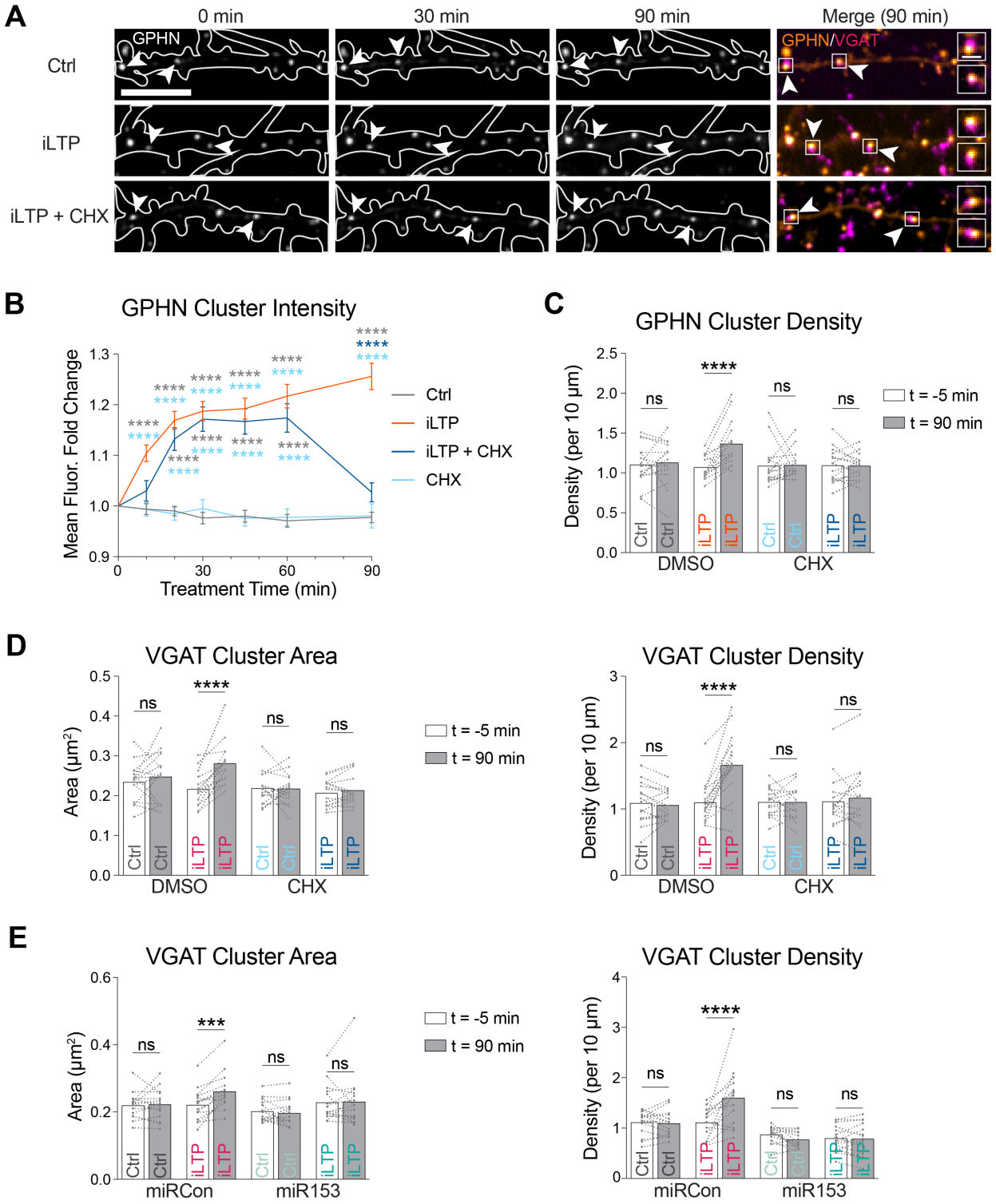

Figure S5. Supplement to Figure 5

(A) Representative dendritic segments of neurons expressing GPHN IB and labeled with an antibody to VGAT, imaged over time in control and iLTP conditions in the presence or absence of translational inhibitor cycloheximide (CHX). Puncta are labeled with filled arrowheads when the fluorescence is unchanged and open arrowheads when

fluorescence increases over time. Boxes indicate the fluorescent puncta enlarged in the merged images (dendrite scale bar, 10 μm; synapse scale bar, 2 μm).

(B) Quantification of fold change in GPHN puncta fluorescence intensity over time following treatment in neurons from A). n = 15 neurons per condition, 10 puncta per neuron.

(C) Paired measurements of GPHN cluster density in dendrites prior to (-5 min) and 90 min following treatment. n = 15 neurons per condition.

(D) Paired measurements of VGAT cluster area (left) and density (right) in dendrites prior to (-5 min) and 90 min following treatment. n = 15 neurons per condition.

(E) Paired measurements of VGAT cluster area (left) and density (right) in miRCon or miR153 OE neurons (as seen in Figure 5A) prior to (-5 min) and 90 min following treatment. n = 15 neurons per condition.

All values represent mean ± SEM. *p<0.05 and **p<0.01, ***p<0.005, ****p<0.0001; RM two-way ANOVA with Geisser-Greenhouse correction (B) and Šidák's multiple comparisons post-hoc test.

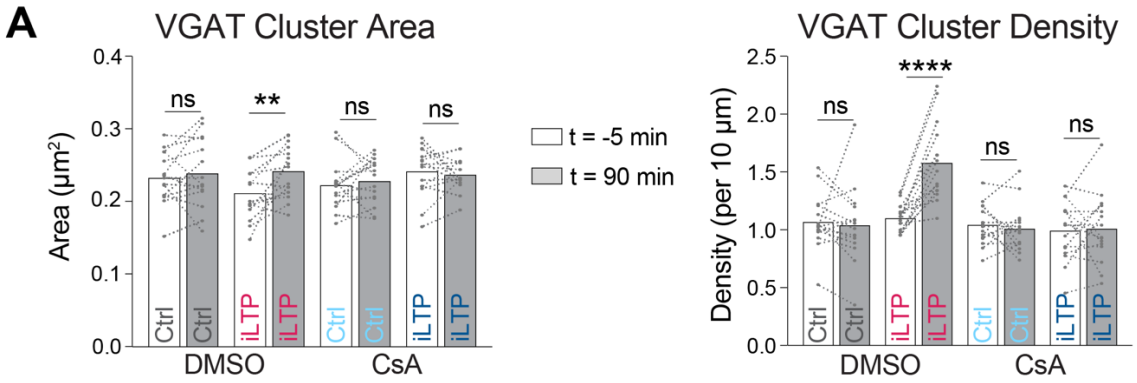

Figure S6. Supplement to Figure 6

(A) Paired measurements of VGAT cluster area (left) and density (right) in treated neurons (as seen in Figure 6D) prior to (-5 min) and 90 min following treatment. n = 15 neurons per condition.

All values represent mean ± SEM. *p<0.05 and **p<0.01, ***p<0.005, ****p<0.0001; RM two-way ANOVA with Šidák's multiple comparisons post-hoc test.

MATERIALS & METHODS

Dissociated hippocampal cultures. Rat hippocampal neurons were dissected from rats (postnatal day 1-2) and prepared as previously described (Crosby et al., 2019). Briefly, hippocampi were disassociated in papain, and neurons were seeded onto coverslips or dishes coated with poly-D-lysine. Neuron density for 18 mm glass coverslips in 12 well plates was 150,000 and 3,000,000 for 6 cm dishes. Neurons were cultured in Neurobasal media (GIBCO) supplemented with B27 (GIBCO) and 2 mM Glutamax. Cells were maintained at 37°C, 5% CO_2 for 14-18 days before experimental use. Half of the neuronal media was replaced with fresh media and anti-mitotics at DIV5, with a subsequent media change at DIV12.

DNA constructs. Adeno associated viruses (AAVs) overexpressing miR153 or scrambled control (miRCon) were purchased from VectorBuilder and used to infect cultured neurons 4 days prior to *in vitro* experiments. The miR153 and miRCon overexpression constructs with GFP expression cassette used in imaging experiments were a gift from Danesh Moazed.[73] Gephyrin-FingR-GFP was a gift from Dr. Don Arnold[50] and Gephyrin-FingR-mScarlet was a gift from Dr. Ulli Bayer.[88] The 3'UTR of *Gphn* and the miR153 upstream sequences were created as gene fragments by Twist Bioscience. The *Gphn* 3'UTR was cloned into the SpeI and MluI restriction sites of pMIR-REPORT, and the miR153 seed site was mutated via site directed mutagenesis (*Gphn* 3'UTR SpeI F: TATATAACTAGTTGACTGTATCCTGTCATATGC, *Gphn* 3'UTR MluI R: CGTATAACGCGTTTTTTAAATAATGATCAAGG, *Gphn* 3'UTR 153 Mut F: GACTGTATCCTGTCACAGGTATCGGCACAGCTAG, *Gphn* 3'UTR 153 Mut R: CTAGCTGTGCCGATACCTGTGACAGGATACAGTC). miR153 upstream sequence was cloned into SacI and HindIII sites (miR153 Upstream Seq SacI F: TATATA GAGCTC TGCGCAGGACCCAGCAGC, miR153 Upstream Seq HindIII R: TATATAAAGCTTCTAAGTAGCTGGCAAAGT) of promoter-less pGL4.10 Firefly luciferase construct (Promega), and the NFAT binding site mutated via site directed mutagenesis (miR153 NFAT Mut F: CACCTCTTGCTGTGTGCGATGCATCCACTAACG, miR153 NFAT Mut R: CGTTAGTGGATGCATCGCACACAGCAAGAGGTG). NFAT knockdown constructs were generated using oligonucleotides based on previously validated NFATc3 mRNA target sequences, [89,90] which were then subcloned into pmU6-[shRNA] ('pSilencer').

Transfections. DIV 12-14 hippocampal neurons were transfected with plasmid DNA and/or miRDIAN miRNA inhibitors (Horizon) using Lipofectamine 2000 (Invitrogen) and used for experiments at DIV14-16.

Stereotactic viral injections. Mice bred at the University of Colorado Anschutz from a B6 genetic background were housed in a dedicated animal care facility. This facility was maintained at 35% humidity, 21-23°C, on a 14/10 light/dark cycle, and mice were housed in ventilated cages with same-sex littermates in groups of 2-5. Food and water were provided *ad libitum*. All procedures were conducted in accordance with guidelines approved by the Administrative Panel on Laboratory Animal Care at University of Colorado Anschutz, School of Medicine, accredited by the Association for Assessment and Accreditation of Laboratory Animal Care International. Mice were stereotactically injected with miRCon and miR153 OE viruses at P21 and subsequent electrophysiology experiments were performed 3 weeks later to allow time for viral expression. Animals induced at 5% isoflurane were maintained at 1-2% isoflurane and head fixed to the stereotactic frame (Kopf Instruments). Using a drill held in the stereotaxic frame, small holes were made in the skull and 0.5 µL AAV solution was injected into the CA1 hippocampus using a Nanoject III (Drummond Scientific) at a rate of 0.1 µL/min at coordinates (in mm): anteroposterior -3, mediolateral 3.5, and dorsoventral -3.

Drug treatments. Chemical iLTP was induced in DIV14-18 hippocampal neurons via bath application of 20 μM NMDA and 10 μM CNQX in HBS solution (in mM): 145 NaCl, 2 KCl, 10 HEPES, 2 $CaCl_2$, 2 $MgCl_2$, 10 glucose (pH adjusted to 7.4). iLTP solution was applied for 2 min at 37°C as previously described.[36] Neurons were imaged live, harvested, or fixed at multiple time points following stimulation as specified in the figures and/or figure legends. 5 μM cyclosporin A (Tocris), 5 μM FK506 (Tocris), or 20 μM BAPTA-AM (Tocris) were added to cell media 15 min prior to iLTP induction and left in media post-stimulation throughout live imaging or until harvested. 1 μM trichostatin A (Tocris) was added to cell media 16 h prior to iLTP induction, and 10 μg/mL cycloheximide (Sigma) was added to bath media and conditioned media throughout live imaging.

RNA isolation and qRT-PCR. RNA was isolated from neurons using the RNeasy mini kit (QIAGEN), and miRNA and mRNA were reverse transcribed into cDNA with the miScript II RT kit (QIAGEN) both according to manufacturer instructions. 1 μL cDNA (diluted 1:10 in RNAase-free water, except when measuring pri-miRNA levels) was used in each qPCR reaction. miRNA-specific primers and the universal primer provided with the miSCript II RT kit or gene-specific primers were used for qPCR in a Biorad CFX384 real time qPCR system. When quantifying pri- or mature miR153 levels over time, we used miR15a or miR410 expression time course data as controls as we have previously shown that iLTP stimulation does not alter these miRNA levels in neurons.[10] qPCR readings were normalized to the U6 snRNA or *Gapdh* mRNA (*Nfactc3*), with U6 primers included in the miScript II RT kit (QIAGEN) and *Gapdh* primers provided by Integrated DNA Technologies. AGO2-bound mRNAs were normalized to respective inputs. Each qPCR run included 40 cycles with parameters: 94°C for 15 min, 55°C for 30 s, and 70°C for 30 s.
Primers. miR153 F: TTGCATAGTCACAAAAGTGATC; miR15a F: TAGCAGCACATAATGGTTT; miR410 F: AATATAACACAG; Pri-153 F: AGCGGTGGCCAGTGTCATT; Pri-153 R: CACAGTTTCCAATGATCAC; Pri-410 F: TGCTCCGGTCAACACTGGGT; Pri-410 R: AAAACAGGCCATCTGTGTTA; *Gphn* F: GGAGACAACCCAGATGACTTAC; *Gphn* R: CCAGCACCTGCTTGAGATAG; *Nfatc3* F: TGGCATCAACAGTATGGACCTGGA; *Nfatc3* R: TTTACCACAAGGAGAAGTGGGCCT; *Gapdh* F: GATGCTGGTGCTGAGTATGT; *Gapdh* R: GCTGACAATCTTGAGGGAGTT.

Luciferase assays. DIV12-14 hippocampal neurons or HEK293T cells plated in 12 well dishes were co-transfected with 500 μg each of Renilla luciferase construct and the appropriate Firefly luciferase reporter construct. miRCon or miR153 were co-transfected when appropriate. Dual-luciferase reporter assays (Promega) were performed according to manufacturer instructions, and Firefly activity was normalized to Renilla activity.

Western blotting. Cells were scraped in 2x protein loading buffer: 4% SDS, 20% glycerol, 120 mM Tris at pH 6.8, 0.02% bromophenol blue, 5% 2-mercaptoethanol. Extracts were then boiled for 5 min at 95°C and proteins were resolved using SDS-PAGE. Wet transfer apparatus was used to transfer proteins to PVDF membranes which were then blocked with 5% milk solution in PBS-Tween. Membranes were incubated at 4°C overnight with the appropriate primary antibody: GPHN (1:5000 Synaptic Systems 147111), $GABA_AR\alpha1$ (1:1000 NeuroMab 75136), $GABA_AR\gamma2$ (1:1000 NeuroMab 75442), GAPDH (1:10,000 GeneTex 627408), GFP (1:2000 NeuroMab 75131), $GABA_AR$ β3 (1:1000 NeuroMab 75149), $GABA_AR\alpha5$ (1:1000 NeuroMab 455510), GLUA1 (1:1000 Millipore ABN241). Membranes were then washed with PBS-Tween and incubated with the appropriate HRP conjugated secondary antibody for 1 hr at room temperature (1:10,000 Millipore). When appropriate, membranes were stripped with stripping

buffer and re-probed. ECL western blotting substrates (Millipore) were used to visualize protein bands and images were analyzed using ImageJ to obtain densitometry measurements. The integrated density of the protein band of interest was normalized to that of GAPDH in the same gel.

Immunofluorescence microscopy. For surface staining, hippocampal neurons on coverslips were fixed with a 4% paraformaldehyde / 4% sucrose solution in PBS for 5 min at room temperature, followed by PBS washes. After incubating in blocking solution (3% bovine serum albumin, 2% normal goat serum in PBS) for 40 min at room temperature, coverslips were surface stained for $GABA_AR\gamma2$ (1:500, Synaptic Systems 224004) or GluA2 (1:200, Invitrogen 32-0300). After surface labeling, neurons were permeabilized with 0.5% NP-40 for 2-3 min and blocked for 40 min prior to GPHN (1:500, Synaptic Systems 147011), VGAT (1:1000, Synaptic Systems 131003), or VGLUT1 (1:1000, Synaptic Systems 135302) staining. All primary antibodies were diluted in blocking solution, and incubations were as follows: $GABA_AR\gamma2$, GPHN, and VGAT for 1 hr at room temperature; GluA2 for 3 hr at room temperature; VGLUT1 overnight at 4°C. Coverslips were then washed 3 x 5 min in PBS and incubated with appropriate secondary antibodies for 1 hr at room temperature (1:1000, ThermoFisher Alexa-Fluor 488, 568, 647). After mounting coverslips onto microscope slides with ProLong gold mounting media (ThermoFisher), confocal images were acquired using: an Axio Observer microscope (Zeiss) equipped with a Tokogawa CSU-X1 spinning disk unit, an EC Plan-Neofluar 63x Plan-Apo (1.4 NA) oil immersion objective lens, a Photometrics Evolve 512 EMCCD camera with 16-bit dynamic range, and SlideBook 6.0 software (3i). Images were acquired using 488, 561, and 640 nm laser excitation to capture 3.96 µm z-stacks (13 xy planes, 0.33 µm intervals) in each channel. The maximum intensity of these planes was projected onto 2D images. The cluster area and density of fluorescent puncta in randomly selected dendrites were analyzed using ImageJ, based on a minimum cluster area threshold of 0.05 μm^2.

Whole cell electrophysiology.
In vitro. DIV18-20 pyramidal hippocampal neurons expressing GFP were patched in whole-cell mode in an extracellular ACSF solution containing (in mM): 10 HEPES, 130 NaCl, 5 KCl, 30 D-glucose, 2 $CaCl_2$, and 1 $MgCl_2$ equilibrated with 95% O_2 / 5% CO_2. mIPSCs were isolated using 2 µM TTX, 100 µM APV, and 10 µM NBQX. Dissociated neurons were held at -70 mV 2 min prior to recording 2 min of continuous activity using an internal solution containing (in mM): 67.5 CsCl, 67.5 $CsMeSO_4$, 0.1 $CaCl_2$, 2 $MgCl_2$, 10 HEPES, 0.1 EGTA, 0.5 Na_3GTP, 3 Na_2ATP, 10 phosphocreatine (pH adjusted to 7.25 with CsOH). Data were collected with a Multiclamp 700b amplifier and digitized with a National Instruments DAQ board at 10 kHz (filtered at 2 kHz, single pole Bessel filter). mIPSCs were quantified using MiniAnalysis software (Synaptosoft Inc.).
Ex vivo. Animals anesthetized with isoflurane were decapitated and their brains rapidly dissected. Horizontal slices (240 µm) were sectioned with a vibratome (Leica VT1200) in cutting solution (in mM): 75 NaCl, 2.5 KCl, 6 MgCl2, 0.1 CaCl2, 1.2 NaH2PO4, 25 NaHCO3, 2.5 D-glucose, 50 sucrose. Slices were then incubated for 30 min in 31.5°C oxygenated ACSF (in mM): 126 NaCl, 2.5 KCl, 1.2 MgCl2, 2.5 CaCl2, 1.2 NaH2PO4, 21.4 NaHCO3, 11.1 D-glucose, also with 10 uM DNQX and 0.5 uM TTX. Tissue recovered at room temperature for at least 1 hour prior to whole-cell patch clamp recordings. Cells were voltage-clamped at -70 mV using 4-6 MΩ patch pipettes in 29.5°C ACSF. All recordings were acquired with Axopatch 200B Amplifiers (Molecular Devices) and Axograph X (Axograph Scientific). mIPSC analysis was performed with Axograph X.

Live imaging. Cultured hippocampal neurons were transfected with Gephyrin-FingR-GFP or co-transfected with Gephyrin-FingR-mScarlet and GFP-tagged miRNA constructs 48-72 hr prior to live imaging experiments. Coverslips were incubated with VGAT-$Oyster^{650}$ antibody (1:200,

Synaptic Systems 131103C5) in conditioned media for 20 min at 37°C. After mounting coverslips in a Ludin chamber with 37°C HBS solution, transfected pyramidal neurons were imaged pre-stimulation (t = 0 min) and then at multiple timepoints 10-90 min following drug treatments in warmed HBS. Confocal images were acquired using the same spinning disk confocal equipment described for fixed immunofluorescent imaging. Images were acquired using 488, 561, and 640 nm laser excitation to capture 3.96 µm z-stacks (13 xy planes, 0.33 µm intervals) in each channel. The maximum intensity of these planes was projected onto 2D images. Fluorescent GPHN puncta co-localized with VGAT were randomly selected in dendrites and their background-subtracted mean fluorescence intensity at each timepoint was measured with ImageJ. The cluster area of VGAT and density of GPHN and VGAT fluorescent puncta in randomly selected dendrites were analyzed using ImageJ, based on a minimum cluster area threshold of 0.05 μm^2.

Acetyl-histone H3 chromatic immunoprecipitation (ChIP). Acetyl-Histone H3 ChIP experiments utilized the EpiQuik Acetyl-Histone H3 ChIP kit (EpiGenetek) and were performed according to manufacturer instructions. DNA eluted from the IP was normalized to input DNA with qPCR using forward and reverse primers (miR153 Upstream Seq F: GGGTTCTAGTCTCGGAACAATAG, miR153 Upstream Seq R: GGGCTCTGGCAACAGTTAAT) targeting the miR153 upstream sequence.

AGO2 RNA immunoprecipitation (IP). Hippocampal neurons were lysed in 1 mL lysis buffer (in mM, unless otherwise specified): 10 HEPES at pH 7.4, 200 NaCl, 30 EDTA, 0.5% Triton X-100, 0.5 U/µL SUPERase inhibitor, 1x Complete Protease Inhibitor. Lysates were then briefly sonicated for 10 s and left on ice for 10 min. Cell debris was pelleted with centrifugation (13,000 rpm for 10 min, 4°C) and 50 µL was taken as protein input while the remaining lysate was pre-cleared using 100 µL or Protein G Sepharose beads (Sigma) at 4°C for 30 min. After pelleting the beads, remaining lysate was equally divided and incubated with 2 µg Pan-Ago (Millipore; 2A8) or IgG (Cell Signaling 5415) at 4°C for 1 hr. Lysates were incubated with beads at 4°C for 1 hr to capture antibody complexes, and then washed 5 times in 1 mL of lysis buffer. 25% of the purified complex was boiled in protein loading buffer followed by western blotting to quantify AGO2 enrichment, and the remaining immunoprecipitate was used for RNA isolation.

Quantification and Statistical Analysis. Every experiment was performed independently at least three times to ensure rigor and reproducibility. All statistical tests were performed in Prism10 (GraphPad). Statistical significance between two groups was determined using t-tests (parametric data) or Mann-Whitney tests (non-parametric). To determine statistical significance between 3 or more groups with a single variable, one-way ANOVA (parametric) or Kruskal-Wallis (non-parametric) and post-hoc multiple comparison tests were used. For unpaired fold change measurements without control error-correction, one-sample t-tests (acceptable data skewness/kurtosis, no outliers) or Wilcoxon signed rank tests were used to compare experimental values against the hypothetical value (1.0) to determine statistical significance. For experiments with 2 variables, statistical significance was determined using ordinary (unpaired) or repeated measures (RM, paired data) two-way ANOVA with post-hoc multiple comparison tests. Exact sample sizes and statistical tests used to determine significance for each experiment are specified in the figure legends. P-values were considered significant if < 0.05. Error bars on all quantification graphs represent the standard error of the mean (SEM).

ACKNOWLEDGEMENTS

This work was supported by NIMH grants R01MH119154 and R01MH128199 to K.R.S., NINDS institutional research training grant 5T32NS099042 and Ruth L. Kirschstein individual predoctoral National Research Service Award (NRSA) F31NS12410 to T.M.W., NINDS Blueprint Diversity Specialized Predoctoral to Postdoctoral Advancement in Neuroscience (D-SPAN) Award (FNS120640A) to J.D.G., NINDS individual predoctoral NRSA F31NS130979 to D.J.K., NIDA individual predoctoral NRSA for MD/PhD (F30DA048543) to S.M.Z., NIMH grant R01MH123700 to M.L.D., NINDS grant R35NS116879 to M.J.K., NIDA grant R01DA35821 and NINDS grant R01NS95809 to C.P.F. Contents are the authors' sole responsibility and do not necessarily represent official NIH views.

REFERENCES

1) Takeuchi T, Duszkiewicz AJ, Morris RG. The synaptic plasticity and memory hypothesis: encoding, storage and persistence. Philos Trans R Soc Lond B Biol Sci. 2013 Dec 2;369(1633):20130288. doi: 10.1098/rstb.2013.0288. PMID: 24298167; PMCID: PMC3843897.
2) Akhondzadeh S. Hippocampal synaptic plasticity and cognition. J Clin Pharm Ther. 1999 Aug;24(4):241-8. doi: 10.1046/j.1365-2710.1999.00231.x. PMID: 10475982.
3) Martin KC, Casadio A, Zhu H, Yaping E, Rose JC, Chen M, Bailey CH, Kandel ER. Synapse-specific, long-term facilitation of aplysia sensory to motor synapses: a function for local protein synthesis in memory storage. Cell. 1997 Dec 26;91(7):927-38. doi: 10.1016/s0092-8674(00)80484-5. PMID: 9428516.
4) Sidrauski C, Acosta-Alvear D, Khoutorsky A, et al. Pharmacological brake-release of mRNA translation enhances cognitive memory. Elife. 2013 May;2:e00498. DOI: 10.7554/elife.00498. PMID: 23741617; PMCID: PMC3667625.
5) Gal-Ben-Ari S, Kenney JW, Ounalla-Saad H, Taha E, David O, Levitan D, Gildish I, Panja D, Pai B, Wibrand K, Simpson TI, Proud CG, Bramham CR, Armstrong JD, Rosenblum K. Consolidation and translation regulation. Learn Mem. 2012 Aug 16;19(9):410-22. doi: 10.1101/lm.026849.112. PMID: 22904372; PMCID: PMC3418764.
6) Laguesse S, Ron D. Protein Translation and Psychiatric Disorders. Neuroscientist. 2020 Feb;26(1):21-42. doi: 10.1177/1073858419853236. Epub 2019 Jul 4. PMID: 31271100; PMCID: PMC7255087.
7) Sutton MA, Schuman EM. Dendritic protein synthesis, synaptic plasticity, and memory. Cell. 2006 Oct 6;127(1):49-58. doi: 10.1016/j.cell.2006.09.014. PMID: 17018276.
8) Klann E, Antion MD, Banko JL, Hou L. Synaptic plasticity and translation initiation. Learning & Memory. 2004 Jul 1;11(4):365-72.
9) Rosenberg T, Gal-Ben-Ari S, Dieterich DC, Kreutz MR, Ziv NE, Gundelfinger ED, Rosenblum K. The roles of protein expression in synaptic plasticity and memory consolidation. Front Mol Neurosci. 2014 Nov 12;7:86. doi: 10.3389/fnmol.2014.00086. PMID: 25429258; PMCID: PMC4228929.
10) Rajgor D, Purkey AM, Sanderson JL, Welle TM, Garcia JD, Dell'Acqua ML, Smith KR. Local miRNA-Dependent Translational Control of GABAAR Synthesis during Inhibitory Long-Term Potentiation. Cell Rep. 2020 Jun 23;31(12):107785. doi: 10.1016/j.celrep.2020.107785. PMID: 32579917; PMCID: PMC7486624.
11) Rajgor D, Welle TM, Smith KR. The Coordination of Local Translation, Membranous Organelle Trafficking, and Synaptic Plasticity in Neurons. Front Cell Dev Biol. 2021 Jul 14;9:711446. doi: 10.3389/fcell.2021.711446. PMID: 34336865; PMCID: PMC8317219.
12) Costa-Mattioli M, Sossin WS, Klann E, Sonenberg N. Translational control of long-lasting synaptic plasticity and memory. Neuron. 2009 Jan 15;61(1):10-26. doi: 10.1016/j.neuron.2008.10.055. PMID: 19146809; PMCID: PMC5154738.
13) Cajigas IJ, Will T, Schuman EM. Protein homeostasis and synaptic plasticity. EMBO J. 2010 Aug 18;29(16):2746-52. doi: 10.1038/emboj.2010.173. PMID: 20717144; PMCID: PMC2924649.

14) Klausberger T, Somogyi P. Neuronal diversity and temporal dynamics: the unity of hippocampal circuit operations. Science. 2008 Jul 4;321(5885):53-7. doi: 10.1126/science.1149381. PMID: 18599766; PMCID: PMC4487503.
15) Chiu CQ, Barberis A, Higley MJ. Preserving the balance: diverse forms of long-term GABAergic synaptic plasticity. Nat Rev Neurosci. 2019 May;20(5):272-281. doi: 10.1038/s41583-019-0141-5. PMID: 30837689.
16) Lorenz-Guertin JM, Jacob TC. GABA type a receptor trafficking and the architecture of synaptic inhibition. Dev Neurobiol. 2018 Mar;78(3):238-270. doi: 10.1002/dneu.22536. Epub 2017 Sep 19. PMID: 28901728; PMCID: PMC6589839.
17) Tyagarajan SK, Fritschy JM. Gephyrin: a master regulator of neuronal function? Nat Rev Neurosci. 2014 Mar;15(3):141-56. doi: 10.1038/nrn3670. PMID: 24552784.
18) Tretter V, Jacob TC, Mukherjee J, Fritschy JM, Pangalos MN, Moss SJ. The clustering of GABA(A) receptor subtypes at inhibitory synapses is facilitated via the direct binding of receptor alpha 2 subunits to gephyrin. J Neurosci. 2008 Feb 6;28(6):1356-65. doi: 10.1523/JNEUROSCI.5050-07.2008. PMID: 18256255; PMCID: PMC6671568.
19) Tretter V, Kerschner B, Milenkovic I, Ramsden SL, Ramerstorfer J, Saiepour L, Maric HM, Moss SJ, Schindelin H, Harvey RJ, Sieghart W, Harvey K. Molecular basis of the γ-aminobutyric acid A receptor α3 subunit interaction with the clustering protein gephyrin. J Biol Chem. 2011 Oct 28;286(43):37702-11. doi: 10.1074/jbc.M111.291336. Epub 2011 Aug 31. PMID: 21880742; PMCID: PMC3199513.
20) Mukherjee J, Kretschmannova K, Gouzer G, Maric HM, Ramsden S, Tretter V, Harvey K, Davies PA, Triller A, Schindelin H, Moss SJ. The residence time of GABA(A)Rs at inhibitory synapses is determined by direct binding of the receptor α1 subunit to gephyrin. J Neurosci. 2011 Oct 12;31(41):14677-87. doi: 10.1523/JNEUROSCI.2001-11.2011. PMID: 21994384; PMCID: PMC3202462.
21) Fritschy JM, Harvey RJ, Schwarz G. Gephyrin: where do we stand, where do we go? Trends Neurosci. 2008 May;31(5):257-64. doi: 10.1016/j.tins.2008.02.006. Epub 2008 Apr 9. PMID: 18403029.
22) Mele M, Costa RO, Duarte CB. Alterations in GABAA-Receptor Trafficking and Synaptic Dysfunction in Brain Disorders. Front Cell Neurosci. 2019 Mar 7;13:77. doi: 10.3389/fncel.2019.00077. PMID: 30899215; PMCID: PMC6416223.
23) Smith KR, Kittler JT. The cell biology of synaptic inhibition in health and disease. Curr Opin Neurobiol. 2010 Oct;20(5):550-6. doi: 10.1016/j.conb.2010.06.001. Epub 2010 Jul 23. PMID: 20650630.
24) Dejanovic B, Lal D, Catarino CB, Arjune S, Belaidi AA, Trucks H, Vollmar C, Surges R, Kunz WS, Motameny S, Altmüller J, Köhler A, Neubauer BA, Epicure Consortium, Nürnberg P, Noachtar S, Schwarz G, Sander T. Exonic microdeletions of the gephyrin gene impair GABAergic synaptic inhibition in patients with idiopathic generalized epilepsy. Neurobiol Dis. 2014 Jul;67:88-96. doi: 10.1016/j.nbd.2014.02.001. Epub 2014 Feb 19. PMID: 24561070.
25) Dejanovic B, Djémié T, Grünewald N, Suls A, Kress V, Hetsch F, Craiu D, Zemel M, Gormley P, Lal D; EuroEPINOMICS Dravet working group; Myers CT, Mefford HC, Palotie A, Helbig I, Meier JC, De Jonghe P, Weckhuysen S, Schwarz G. Simultaneous impairment of neuronal and metabolic function of mutated gephyrin in a patient with epileptic encephalopathy. EMBO Mol Med. 2015 Dec;7(12):1580-94. doi: 10.15252/emmm.201505323. Erratum in: EMBO Mol Med. 2017 Dec;9(12):1764. PMID: 26613940; PMCID: PMC4693503.
26) González MI. The possible role of GABAA receptors and gephyrin in epileptogenesis. Front Cell Neurosci. 2013 Jul 22;7:113. doi: 10.3389/fncel.2013.00113. PMID: 23885234; PMCID: PMC3717475.
27) Fang M, Shen L, Yin H, Pan YM, Wang L, Chen D, Xi ZQ, Xiao Z, Wang XF, Zhou SN. Downregulation of gephyrin in temporal lobe epilepsy neurons in humans and a rat model. Synapse. 2011 Oct;65(10):1006-14. doi: 10.1002/syn.20928. Epub 2011 Apr 7. PMID: 21404332.
28) Agarwal S, Tannenberg RK, Dodd PR. Reduced expression of the inhibitory synapse scaffolding protein gephyrin in Alzheimer's disease. J Alzheimers Dis. 2008 Jul;14(3):313-21. doi: 10.3233/jad-2008-14305. PMID: 18599957.

29) Hales CM, Rees H, Seyfried NT, Dammer EB, Duong DM, Gearing M, Montine TJ, Troncoso JC, Thambisetty M, Levey AI, Lah JJ, Wingo TS. Abnormal gephyrin immunoreactivity associated with Alzheimer disease pathologic changes. J Neuropathol Exp Neurol. 2013 Nov;72(11):1009-15. doi: 10.1097/01.jnen.0000435847.59828.db. PMID: 24128675; PMCID: PMC4037931.
30) Kiss E, Gorgas K, Schlicksupp A, Groß D, Kins S, Kirsch J, Kuhse J. Biphasic Alteration of the Inhibitory Synapse Scaffold Protein Gephyrin in Early and Late Stages of an Alzheimer Disease Model. Am J Pathol. 2016 Sep;186(9):2279-91. doi: 10.1016/j.ajpath.2016.05.013. Epub 2016 Jul 14. PMID: 27423698.
31) Barberis A. Postsynaptic plasticity of GABAergic synapses. Neuropharmacology. 2020 Jun 1;169:107643. doi: 10.1016/j.neuropharm.2019.05.020. Epub 2019 May 17. PMID: 31108109.
32) Bloss EB, Cembrowski MS, Karsh B, Colonell J, Fetter RD, Spruston N. Structured Dendritic Inhibition Supports Branch-Selective Integration in CA1 Pyramidal Cells. Neuron. 2016 Mar 2;89(5):1016-30. doi: 10.1016/j.neuron.2016.01.029. Epub 2016 Feb 18. PMID: 26898780.
33) Bar-Ilan L, Gidon A, Segev I. The role of dendritic inhibition in shaping the plasticity of excitatory synapses. Front Neural Circuits. 2013 Apr 3;6:118. doi: 10.3389/fncir.2012.00118. PMID: 23565076; PMCID: PMC3615258.
34) Marsden KC, Beattie JB, Friedenthal J, Carroll RC. NMDA receptor activation potentiates inhibitory transmission through GABA receptor-associated protein-dependent exocytosis of GABA(A) receptors. J Neurosci. 2007 Dec 26;27(52):14326-37. doi: 10.1523/JNEUROSCI.4433-07.2007. PMID: 18160640; PMCID: PMC6673443.
35) Marsden KC, Shemesh A, Bayer KU, Carroll RC. Selective translocation of Ca2+/calmodulin protein kinase IIalpha (CaMKIIalpha) to inhibitory synapses. Proc Natl Acad Sci U S A. 2010 Nov 23;107(47):20559-64. doi: 10.1073/pnas.1010346107. Epub 2010 Nov 8. PMID: 21059908; PMCID: PMC2996683.
36) Petrini EM, Ravasenga T, Hausrat TJ, Iurilli G, Olcese U, Racine V, Sibarita JB, Jacob TC, Moss SJ, Benfenati F, Medini P, Kneussel M, Barberis A. Synaptic recruitment of gephyrin regulates surface GABAA receptor dynamics for the expression of inhibitory LTP. Nat Commun. 2014 Jun 4;5:3921. doi: 10.1038/ncomms4921. PMID: 24894704; PMCID: PMC4059940.
37) Chiu CQ, Martenson JS, Yamazaki M, Natsume R, Sakimura K, Tomita S, Tavalin SJ, Higley MJ. Input-Specific NMDAR-Dependent Potentiation of Dendritic GABAergic Inhibition. Neuron. 2018 Jan 17;97(2):368-377.e3. doi: 10.1016/j.neuron.2017.12.032. PMID: 29346754; PMCID: PMC5777295.
38) Williams LE, Holtmaat A. Higher-Order Thalamocortical Inputs Gate Synaptic Long-Term Potentiation via Disinhibition. Neuron. 2019 Jan 2;101(1):91-102.e4. doi: 10.1016/j.neuron.2018.10.049. Epub 2018 Nov 21. PMID: 30472077.
39) Leão RN, Mikulovic S, Leão KE, Munguba H, Gezelius H, Enjin A, Patra K, Eriksson A, Loew LM, Tort AB, Kullander K. OLM interneurons differentially modulate CA3 and entorhinal inputs to hippocampal CA1 neurons. Nat Neurosci. 2012 Nov;15(11):1524-30. doi: 10.1038/nn.3235. Epub 2012 Oct 7. PMID: 23042082; PMCID: PMC3483451.
40) Udakis M, Pedrosa V, Chamberlain SEL, Clopath C, Mellor JR. Interneuron-specific plasticity at parvalbumin and somatostatin inhibitory synapses onto CA1 pyramidal neurons shapes hippocampal output. Nat Commun. 2020 Sep 2;11(1):4395. doi: 10.1038/s41467-020-18074-8. PMID: 32879322; PMCID: PMC7467931.
41) Kannan M, Gross GG, Arnold DB, Higley MJ. Visual Deprivation During the Critical Period Enhances Layer 2/3 GABAergic Inhibition in Mouse V1. J Neurosci. 2016 Jun 1;36(22):5914-9. doi: 10.1523/JNEUROSCI.0051-16.2016. PMID: 27251614; PMCID: PMC4887562.
42) Smalheiser NR, Lugli G. microRNA regulation of synaptic plasticity. Neuromolecular Med. 2009;11(3):133-40. doi: 10.1007/s12017-009-8065-2. Epub 2009 May 21. PMID: 19458942; PMCID: PMC3732454.

43) Hu Z, Li Z. miRNAs in synapse development and synaptic plasticity. Curr Opin Neurobiol. 2017 Aug;45:24-31. doi: 10.1016/j.conb.2017.02.014. Epub 2017 Mar 21. PMID: 28334640; PMCID: PMC5554733.
44) Reza-Zaldivar EE, Hernández-Sápiens MA, Minjarez B, Gómez-Pinedo U, Sánchez-González VJ, Márquez-Aguirre AL, Canales-Aguirre AA. Dendritic Spine and Synaptic Plasticity in Alzheimer's Disease: A Focus on MicroRNA. Front Cell Dev Biol. 2020 May 5;8:255. doi: 10.3389/fcell.2020.00255. PMID: 32432108; PMCID: PMC7214692.
45) Im HI, Kenny PJ. MicroRNAs in neuronal function and dysfunction. Trends Neurosci. 2012 May;35(5):325-34. doi: 10.1016/j.tins.2012.01.004. Epub 2012 Mar 19. PMID: 22436491; PMCID: PMC3565236.
46) Lewis BP, Shih IH, Jones-Rhoades MW, Bartel DP, Burge CB. Prediction of mammalian microRNA targets. Cell. 2003 Dec 26;115(7):787-98. doi: 10.1016/s0092-8674(03)01018-3. PMID: 14697198.
47) Wong N, Wang X. miRDB: an online resource for microRNA target prediction and functional annotations. Nucleic Acids Res. 2015 Jan;43(Database issue):D146-52. doi: 10.1093/nar/gku1104. Epub 2014 Nov 5. PMID: 25378301; PMCID: PMC4383922.
48) Hu Z, Yu D, Gu QH, Yang Y, Tu K, Zhu J, Li Z. miR-191 and miR-135 are required for long-lasting spine remodelling associated with synaptic long-term depression. Nat Commun. 2014;5:3263. doi: 10.1038/ncomms4263. PMID: 24535612; PMCID: PMC3951436.
49) Xu, J., Liao, X., Lu, N., Liu, W. and Wong, C.-W. (2011), Chromatin-modifying drugs induce miRNA-153 expression to suppress Irs-2 in glioblastoma cell lines. Int. J. Cancer, 129: 2527-2531. https://doi.org/10.1002/ijc.25917
50) Gross GG, Junge JA, Mora RJ, Kwon HB, Olson CA, Takahashi TT, Liman ER, Ellis-Davies GC, McGee AW, Sabatini BL, Roberts RW, Arnold DB. Recombinant probes for visualizing endogenous synaptic proteins in living neurons. Neuron. 2013 Jun 19;78(6):971-85. doi: 10.1016/j.neuron.2013.04.017. PMID: 23791193; PMCID: PMC3779638.
51) Crosby KC, Gookin SE, Garcia JD, Hahm KM, Dell'Acqua ML, Smith KR. Nanoscale Subsynaptic Domains Underlie the Organization of the Inhibitory Synapse. Cell Rep. 2019 Mar 19;26(12):3284-3297.e3. doi: 10.1016/j.celrep.2019.02.070. PMID: 30893601; PMCID: PMC6529211.
52) Soutschek M, Schratt G. Non-coding RNA in the wiring and remodeling of neural circuits. Neuron. 2023 Jul 19;111(14):2140-2154. doi: 10.1016/j.neuron.2023.04.031. Epub 2023 May 24. PMID: 37230080.
53) Ule J, Jensen KB, Ruggiu M, Mele A, Ule A, Darnell RB. CLIP identifies Nova-regulated RNA networks in the brain. Science. 2003 Nov 14;302(5648):1212-5. doi: 10.1126/science.1090095. PMID: 14615540.
54) Sharangdhar T, Sugimoto Y, Heraud-Farlow J, Fernández-Moya SM, Ehses J, Ruiz de Los Mozos I, Ule J, Kiebler MA. A retained intron in the 3'-UTR of *Calm3* mRNA mediates its Staufen2- and activity-dependent localization to neuronal dendrites. EMBO Rep. 2017 Oct;18(10):1762-1774. doi: 10.15252/embr.201744334. Epub 2017 Aug 1. PMID: 28765142; PMCID: PMC5623867.
55) Lee JA, Damianov A, Lin CH, Fontes M, Parikshak NN, Anderson ES, Geschwind DH, Black DL, Martin KC. Cytoplasmic Rbfox1 Regulates the Expression of Synaptic and Autism-Related Genes. Neuron. 2016 Jan 6;89(1):113-28. doi: 10.1016/j.neuron.2015.11.025. Epub 2015 Dec 10. PMID: 26687839; PMCID: PMC4858412.
56) Zahr SK, Yang G, Kazan H, Borrett MJ, Yuzwa SA, Voronova A, Kaplan DR, Miller FD. A Translational Repression Complex in Developing Mammalian Neural Stem Cells that Regulates Neuronal Specification. Neuron. 2018 Feb 7;97(3):520-537.e6. doi: 10.1016/j.neuron.2017.12.045. Epub 2018 Jan 27. PMID: 29395907.
57) Schieweck R, Kiebler MA. Posttranscriptional Gene Regulation of the GABA Receptor to Control Neuronal Inhibition. Front Mol Neurosci. 2019 Jun 25;12:152. doi: 10.3389/fnmol.2019.00152. PMID: 31316346; PMCID: PMC6611381.

58) Schieweck R, Riedemann T, Forné I, Harner M, Bauer KE, Rieger D, Ang FY, Hutten S, Demleitner AF, Popper B, Derdak S, Sutor B, Bilban M, Imhof A, Kiebler MA. Pumilio2 and Staufen2 selectively balance the synaptic proteome. Cell Rep. 2021 Jun 22;35(12):109279. doi: 10.1016/j.celrep.2021.109279. PMID: 34161769.
59) Rees MI, Harvey K, Ward H, White JH, Evans L, Duguid IC, Hsu CC, Coleman SL, Miller J, Baer K, Waldvogel HJ, Gibbon F, Smart TG, Owen MJ, Harvey RJ, Snell RG. Isoform heterogeneity of the human gephyrin gene (GPHN), binding domains to the glycine receptor, and mutation analysis in hyperekplexia. J Biol Chem. 2003 Jul 4;278(27):24688-96. doi: 10.1074/jbc.M301070200. Epub 2003 Apr 8. PMID: 12684523.
60) Paarmann I, Schmitt B, Meyer B, Karas M, Betz H. Mass spectrometric analysis of glycine receptor-associated gephyrin splice variants. J Biol Chem. 2006 Nov 17;281(46):34918-25. doi: 10.1074/jbc.M607764200. Epub 2006 Sep 25. PMID: 17001074.
61) Prior P, Schmitt B, Grenningloh G, Pribilla I, Multhaup G, Beyreuther K, Maulet Y, Werner P, Langosch D, Kirsch J, et al. Primary structure and alternative splice variants of gephyrin, a putative glycine receptor-tubulin linker protein. Neuron. 1992 Jun;8(6):1161-70. doi: 10.1016/0896-6273(92)90136-2. PMID: 1319186.
62) Smolinsky B, Eichler SA, Buchmeier S, Meier JC, Schwarz G. Splice-specific functions of gephyrin in molybdenum cofactor biosynthesis. J Biol Chem. 2008 Jun 20;283(25):17370-9. doi: 10.1074/jbc.M800985200. Epub 2008 Apr 14. PMID: 18411266.
63) Bedet C, Bruusgaard JC, Vergo S, Groth-Pedersen L, Eimer S, Triller A, Vannier C. Regulation of gephyrin assembly and glycine receptor synaptic stability. J Biol Chem. 2006 Oct 6;281(40):30046-56. doi: 10.1074/jbc.M602155200. Epub 2006 Aug 1. PMID: 16882665.
64) Saiyed T, Paarmann I, Schmitt B, Haeger S, Sola M, Schmalzing G, Weissenhorn W, Betz H. Molecular basis of gephyrin clustering at inhibitory synapses: role of G- and E-domain interactions. J Biol Chem. 2007 Feb 23;282(8):5625-32. doi: 10.1074/jbc.M610290200. Epub 2006 Dec 20. PMID: 17182610.
65) Dos Reis R, Kornobis E, Pereira A, Tores F, Carrasco J, Gautier C, Jahannault-Talignani C, Nitschké P, Muchardt C, Schlosser A, Maric HM, Ango F, Allemand E. Complex regulation of Gephyrin splicing is a determinant of inhibitory postsynaptic diversity. Nat Commun. 2022 Jun 18;13(1):3507. doi: 10.1038/s41467-022-31264-w. PMID: 35717442; PMCID: PMC9206673.
66) Papadopoulos T, Korte M, Eulenburg V, Kubota H, Retiounskaia M, Harvey RJ, Harvey K, O'Sullivan GA, Laube B, Hülsmann S, Geiger JR, Betz H. Impaired GABAergic transmission and altered hippocampal synaptic plasticity in collybistin-deficient mice. EMBO J. 2007 Sep 5;26(17):3888-99. doi: 10.1038/sj.emboj.7601819. Epub 2007 Aug 9. PMID: 17690689; PMCID: PMC1994120.
67) Schratt GM, Tuebing F, Nigh EA, Kane CG, Sabatini ME, Kiebler M, Greenberg ME. A brain-specific microRNA regulates dendritic spine development. Nature. 2006 Jan 19;439(7074):283-9. doi: 10.1038/nature04367. Erratum in: Nature. 2006 Jun 15;441(7095):902. PMID: 16421561.
68) Sambandan S, Akbalik G, Kochen L, Rinne J, Kahlstatt J, Glock C, Tushev G, Alvarez-Castelao B, Heckel A, Schuman EM. Activity-dependent spatially localized miRNA maturation in neuronal dendrites. Science. 2017 Feb 10;355(6325):634-637. doi: 10.1126/science.aaf8995. PMID: 28183980.
69) Tushev G, Glock C, Heumüller M, Biever A, Jovanovic M, Schuman EM. Alternative 3' UTRs Modify the Localization, Regulatory Potential, Stability, and Plasticity of mRNAs in Neuronal Compartments. Neuron. 2018 May 2;98(3):495-511.e6. doi: 10.1016/j.neuron.2018.03.030. Epub 2018 Apr 12. PMID: 29656876.
70) Donlin-Asp PG, Polisseni C, Klimek R, Heckel A, Schuman EM. Differential regulation of local mRNA dynamics and translation following long-term potentiation and depression. Proc Natl Acad Sci U S A. 2021 Mar 30;118(13):e2017578118. doi: 10.1073/pnas.2017578118. PMID: 33771924; PMCID: PMC8020670.

71) Biever A, Glock C, Tushev G, Ciirdaeva E, Dalmay T, Langer JD, Schuman EM. Monosomes actively translate synaptic mRNAs in neuronal processes. Science. 2020 Jan 31;367(6477):eaay4991. doi: 10.1126/science.aay4991. PMID: 32001627.
72) Biever A, Donlin-Asp PG, Schuman EM. Local translation in neuronal processes. Curr Opin Neurobiol. 2019 Aug;57:141-148. doi: 10.1016/j.conb.2019.02.008. Epub 2019 Mar 9. PMID: 30861464.
73) Mathew RS, Tatarakis A, Rudenko A, Johnson-Venkatesh EM, Yang YJ, Murphy EA, Todd TP, Schepers ST, Siuti N, Martorell AJ, Falls WA, Hammack SE, Walsh CA, Tsai LH, Umemori H, Bouton ME, Moazed D. A microRNA negative feedback loop downregulates vesicle transport and inhibits fear memory. Elife. 2016 Dec 21;5:e22467. doi: 10.7554/eLife.22467. PMID: 28001126; PMCID: PMC5293492.
74) Yan ML, Zhang S, Zhao HM, Xia SN, Jin Z, Xu Y, Yang L, Qu Y, Huang SY, Duan MJ, Mao M, An XB, Mishra C, Zhang XY, Sun LH, Ai J. MicroRNA-153 impairs presynaptic plasticity by blocking vesicle release following chronic brain hypoperfusion. Cell Commun Signal. 2020 Apr 6;18(1):57. doi: 10.1186/s12964-020-00551-8. PMID: 32252776; PMCID: PMC7137307.
75) You YH, Qin ZQ, Zhang HL, Yuan ZH, Yu X. MicroRNA-153 promotes brain-derived neurotrophic factor and hippocampal neuron proliferation to alleviate autism symptoms through inhibition of JAK-STAT pathway by LEPR. Biosci Rep. 2019 Jun 25;39(6):BSR20181904. doi: 10.1042/BSR20181904. PMID: 30975733; PMCID: PMC6591574.
76) Qiao J, Zhao J, Chang S, Sun Q, Liu N, Dong J, Chen Y, Yang D, Ye D, Liu X, Yu Y, Chen W, Zhu S, Wang G, Jia W, Xi J, Kang J. MicroRNA-153 improves the neurogenesis of neural stem cells and enhances the cognitive ability of aged mice through the notch signaling pathway. Cell Death Differ. 2020 Feb;27(2):808-825. doi: 10.1038/s41418-019-0388-4. Epub 2019 Jul 11. PMID: 31296962; PMCID: PMC7206122.
77) Gupta P, Bhattacharjee S, Sharma AR, Sharma G, Lee SS, Chakraborty C. miRNAs in Alzheimer Disease - A Therapeutic Perspective. Curr Alzheimer Res. 2017;14(11):1198-1206. doi: 10.2174/1567205014666170829101016. PMID: 28847283.
78) Bi D, Wen L, Wu Z, Shen Y. GABAergic dysfunction in excitatory and inhibitory (E/I) imbalance drives the pathogenesis of Alzheimer's disease. Alzheimers Dement. 2020 Sep;16(9):1312-1329. doi: 10.1002/alz.12088. Epub 2020 Jun 16. PMID: 32543726.
79) Busche MA, Konnerth A. Impairments of neural circuit function in Alzheimer's disease. Philos Trans R Soc Lond B Biol Sci. 2016 Aug 5;371(1700):20150429. doi: 10.1098/rstb.2015.0429. PMID: 27377723; PMCID: PMC4938029.
80) Yizhar O, Fenno LE, Prigge M, Schneider F, Davidson, TJ, O'Shea, DJ, Sohal VS, Goshen I, Finkelstein J, Paz JT, Stehfest K, Fudim R, Ramakrishnan C, Huguenard JR, Hegemann P, Deisseroth K. Neocortical excitation/inhibition balance in information processing and social dysfunction. *Nature* **477**, 171–178 (2011). https://doi.org/10.1038/nature10360
81) Ferguson BR, Gao WJ. PV Interneurons: Critical Regulators of E/I Balance for Prefrontal Cortex-Dependent Behavior and Psychiatric Disorders. Front Neural Circuits. 2018 May 16;12:37. doi: 10.3389/fncir.2018.00037. PMID: 29867371; PMCID: PMC5964203.
82) Selten M, van Bokhoven H, Nadif Kasri N. Inhibitory control of the excitatory/inhibitory balance in psychiatric disorders. F1000Res. 2018 Jan 8;7:23. doi: 10.12688/f1000research.12155.1. PMID: 29375819; PMCID: PMC5760969.
83) Gao R, Penzes P. Common mechanisms of excitatory and inhibitory imbalance in schizophrenia and autism spectrum disorders. Curr Mol Med. 2015;15(2):146-67. doi: 10.2174/1566524015666150303003028. PMID: 25732149; PMCID: PMC4721588.
84) Krol J, Busskamp V, Markiewicz I, Stadler MB, Ribi S, Richter J, Duebel J, Bicker S, Fehling HJ, Schübeler D, Oertner TG, Schratt G, Bibel M, Roska B, Filipowicz W. Characterizing light-regulated retinal microRNAs reveals rapid turnover as a common property of neuronal microRNAs. Cell. 2010 May 14;141(4):618-31. doi: 10.1016/j.cell.2010.03.039. PMID: 20478254.

85) Sethi P, Lukiw WJ. Micro-RNA abundance and stability in human brain: specific alterations in Alzheimer's disease temporal lobe neocortex. Neurosci Lett. 2009 Aug 7;459(2):100-4. doi: 10.1016/j.neulet.2009.04.052. Epub 2009 May 4. PMID: 19406203.
86) Rüegger S, Großhans H. MicroRNA turnover: when, how, and why. Trends Biochem Sci. 2012 Oct;37(10):436-46. doi: 10.1016/j.tibs.2012.07.002. Epub 2012 Aug 23. PMID: 22921610.
87) Gu QH, Yu D, Hu Z, Liu X, Yang Y, Luo Y, Zhu J, Li Z. miR-26a and miR-384-5p are required for LTP maintenance and spine enlargement. Nat Commun. 2015 Apr 10;6:6789. doi: 10.1038/ncomms7789. PMID: 25858512; PMCID: PMC4403380.
88) Cook SG, Goodell DJ, Restrepo S, Arnold DB, Bayer KU. Simultaneous Live Imaging of Multiple Endogenous Proteins Reveals a Mechanism for Alzheimer's-Related Plasticity Impairment. Cell Rep. 2019 Apr 16;27(3):658-665.e4. doi: 10.1016/j.celrep.2019.03.041. PMID: 30995464; PMCID: PMC6482958.
89) Ulrich JD, Kim MS, Houlihan PR, Shutov LP, Mohapatra DP, Strack S, Usachev YM (2013) Distinct activation properties of the nuclear factor of activated T-cells (NFAT) isoforms NFATc3 and NFATc4 in neurons. J Biol Chem 287:37594-37609.
90) Vashishta A, Habas A, Pruunsild P, Zheng JJ, Timmusk T, Hetman M (2009) Nuclear factor of activated T-cells isoform c4 (NFATc4/NFAT3) as a mediator of antiapoptotic transcription in NMDA receptor-stimulated cortical neurons. J Neurosci 29:15331-15340.